PHASED-COSTAS CODING OF MIMO RADAR WAVEFORMS FOR TRANSMIT BEAMFORMING USING GENERALIZED AMBIGUITY FUNCTIONS

A THESIS SUBMITTED TO
THE GRADUATE SCHOOL OF NATURAL AND APPLIED SCIENCES
OF
MIDDLE EAST TECHNICAL UNIVERSITY

BY

OZAN ONUR ÇELIK

IN PARTIAL FULFILLMENT OF THE REQUIREMENTS
FOR
THE DEGREE OF MASTER OF SCIENCE
IN
ELECTRICAL AND ELECTRONICS ENGINEERING

SEPTEMBER 2021

Approval of the thesis:

PHASED-COSTAS CODING OF MIMO RADAR WAVEFORMS FOR TRANSMIT BEAMFORMING USING GENERALIZED AMBIGUITY FUNCTIONS

submitted by **OZAN ONUR ÇELIK** in partial fulfillment of the requirements for the degree of **Master of Science in Electrical and Electronics Engineering Department, Middle East Technical University** by,

Prof. Dr. Halil Kalıpçılar
Dean, Graduate School of **Natural and Applied Sciences** _____

Prof. Dr. İlkay Ulusoy
Head of Department, **Electrical and Electronics Engineering** _____

Prof. Dr. T. Engin Tuncer
Supervisor, **Electrical & Electronics Engineering, METU** _____

Examining Committee Members:

Prof. Dr. Kemal Leblebicioğlu
Electrical & Electronics Engineering, METU _____

Prof. Dr. T. Engin Tuncer
Electrical & Electronics Engineering, METU _____

Prof. Dr. Orhan Arıkan
Electrical & Electronics Engineering, Bilkent University _____

Prof. Dr. Çağatay Candan
Electrical & Electronics Engineering, METU _____

Prof. Dr. Umut Orguner
Electrical & Electronics Engineering, METU _____

Date: 07.09.2021

I hereby declare that all information in this document has been obtained and presented in accordance with academic rules and ethical conduct. I also declare that, as required by these rules and conduct, I have fully cited and referenced all material and results that are not original to this work.

Name, Surname: Ozan Onur Çelik

Signature :

ABSTRACT

PHASED-COSTAS CODING OF MIMO RADAR WAVEFORMS FOR TRANSMIT BEAMFORMING USING GENERALIZED AMBIGUITY FUNCTIONS

Çelik, Ozan Onur
M.S., Department of Electrical and Electronics Engineering
Supervisor: Prof. Dr. T. Engin Tuncer

September 2021, 78 pages

Multiple-input multiple-output (MIMO) radars have attracted interest due to some important advantages over Phased-array radars. The diversity that comes with multiple waveforms is used to maximize the power in the vicinity of targets and minimize the cross correlation of waveforms reflected from multiple targets for predefined angular sectors. In this study, a novel approach is presented to overcome the limitatons of current beamformer design techniques in terms of bandwidth, auto/cross (spatial) correlations, range-Doppler resolutions, peak-to-average ratio (PAR), and mean squared error (MSE) for desired beamforming pattern. A generalized ambiguity function formulation is presented which employs all the beamformer design parameters in a mathematically tractable simple manner suitable for constrained optimization. We present Phased-Costas coded waveforms to generate desired beampatterns while minimizing range-doppler sidelobes and target cross-correlations with limited bandwidth. Beamformer design problem is casted as a constrained optimization which includes PAR constraint. The resulting NP hard problem with nonconvex objective function is converted to a convex problem and efficiently solved by using ADMM technique in polynomial time. The optimum beamformer solution is shown to achieve $\mathrm{PAR} = 1$ with

very little degradation compared to the unconstrained problem making the ultimate choice for MIMO beamforming applications. Several good features of the designed beamformer are shown through simulations and compared to known methods.

Keywords: MIMO Radar, transmit beampattern, ADMM, Costas codes,space-time coding, generalized ambiguity function, Peak to average ratio (PAR).

ÖZ

GENELLEŞTİRİLMİŞ KARIŞIKLIK FONKSİYONU İLE FAZ-COSTAS KODLU MIMO RADAR DALGABİÇİMLERİNİN HÜZME ŞEKİLLENDİRMESİ

Çelik, Ozan Onur
Yüksek Lisans, Elektrik ve Elektronik Mühendisliği Bölümü
Tez Yöneticisi: Prof. Dr. T. Engin Tuncer

Eylül 2021 , 78 sayfa

Çok-Giriş-Çok-Çıkış (ÇGÇÇ) radarlar Faz-Dizili radarlara göre önemli avantajlar göstermekte olduğu için güncel araştırma konuları arasındadır. Çoklu dalgabiçimi kullanılmasının getirmiş olduğu çeşitlilik gönderilen sinyalleri hedeflerin üzerinde toplamaya ve aynı zamanda farklı açılardaki hedeflerden yansıyan sinyallerin çapraz ilintisini azaltmak üzerine tasarlanabilmektedir. Bu çalışmada, güncel hüzme yönlendirme algoritmalarında karşılaşılan kısıtlar (bantgenişliği, oto- ve çapraz- ilintileri, menzil-Doppler çözünürlükleri, tepe-ortalama güç oranı, ve hüzmenin ortalama kare hatası) göz önünde bulundurularak yeni bir yaklaşım yapılmıştır. Genelleştirişmis karışıklık fonksiyonu oluşturulup tüm tasarım parametrelerini optimizasyona uygun şekilde olacak şekilde ifade edilmiştir. Faz-Costas kodları istenilen hüzmeyi, menzil-Doppler yan lobları ve hedef sinyallerinin ilintinlerini sınırlı bantgenişliği içinde çözme amacıyla kullanılmıştır. Hüzme tasarım problemi tepe-ortalama güç kısıtı göz önünde bulundularak çözülmüştür. Oluşan nonkonveks ve NP zorluklu problem konveks hale çevrilip ADMM metodu ile polinom zamanda çözülebilmektedir.

Eniyilenmiş çözüm PAR=1 kısıtı ile bulunup benzer çalışmalarla karşılaştırılmıştır.

Anahtar Kelimeler: MIMO Radar, hüzmeşekillendirme, ADMM, Costas kodları,Karışıklık fonksiyonu

To Ruzi ...

ACKNOWLEDGMENTS

I would like to thank to my supervisor Prof. T. Engin Tuncer for his guidance, insights and suggestions at every stage of this study. I learned very much from him about research and academic writing. His constant support and motivation helped me a lot to improve myself.

I would like to thank my colleauges at TUBITAK ILTAREN for valuable discussions and friendly enviroment during this study.

I wish to express my deepest gratitude to my family for their care and patience for all the time.

TABLE OF CONTENTS

LIST OF TABLES

TABLES

LIST OF FIGURES

FIGURES

LIST OF ALGORITHMS

ALGORITHMS

LIST OF ABBREVIATIONS

2D	2 Dimensional
3D	3 Dimensional
PCC	Phased-Costas Code
PAR	Peak to Average Ratio
ADMM	Alternating Direction Method of Multipliers
CDF	Cumulative Distribution Function
STFT	Short-Time Fourier Transform
MIMO	Multiple Input Multiple Output
SISO	Single Input Single Output
SINR	Signal to Interference Ratio
CA	Cyclic Adaptive
SQP	Semidefinite Quadratic Programming
GLRT	Generalized Likelihood Ratio Test
RCS	Radar Cross Section
CRB	Cramer-Rao Bound

CHAPTER 1

INTRODUCTION

1.1 Motivation and Problem Definition

MIMO radar has been a topic of intensive research due to some important advantages over phased array radars. It has ability to send uncorrelated waveforms via its antennas unlike phased arrays where only a complex multiple of the same signal is transmitted. This diversity means higher degree of freedom and it is utilized in various ways depending on the placement of its antennas. MIMO radar antennas can be used as widely distributed or colocated, each having its own merits. For the former type, [9] shows that it provides ability to achieve diversity gain and spatial multiplexing. Widely separated MIMO systems, also called distributed MIMO, make use of the spatial diversity of the targets as it is viewed from different angles which enables them to exploit the target in a similar manner where MIMO in communication systems is used to cope with fading channels [10]. For the latter type, [1] shows that MIMO has superiority in the maximum number of identifiable targets, effective use of adaptive methods for target detection and estimation, and flexibility for transmit beampattern design. For colocated MIMO systems, studies show that MIMO performance in terms of resolution improvement [11], moving target detection [12] , parameter identifiability [13] and data-adaptive array techniques [14] are significantly improved.

Studies on MIMO waveform designs have focused on different requirements. Recent works can be classified into two main categories. First objective focuses on signal to interference noise ratio (SINR) maximization which includes the optimization of transmitter and receive filter together with target statistics and interference. [15] proposes an approach to solve sequence of convex quadratically constrained quadratic

programming (QCQP) for the problem of SINR maximization subject to constant modulus and similarity constraints. The solution converges to a suboptimal solution however at each iteration it shows improvement in SINR. [16] proposes waveform design based on maximizing conditional mutual information between target impulse response and reflected waveform assuming second order statistics of targets available. Other information theoretic approaches can be found [17], [18]. [19] uses an iterative algorithm based on cyclic optimization of waveform and receive filter that uses non-decreasing SINR. [20] investigates SINR maximization under signal dependent interference and white Gaussian noise with constant modulus and similarity constraints using two step sequential optimization with relaxation and randomization techniques that jointly optimizes transmit waveforms and receive filters. Another study based on relaxation and randomization can be found in [21]. The similarity constraint in this context is a reference signal to force the optimized signal have similar autocorrelation characteristics. [22] focuses on maximizing SINR of ground moving targets in the presence of clutter using a priori interference statistics with practical constraint such as constant modulus and discrete phase shifts. Other waveform design problems based on SINR maximization have been discussed in [23], [24], [25], [26] under energy constraint, constant modulus constraint or similarity constraint.

The second objective which is also the subject of this thesis is to control the spatial and temporal properties of the transmit signals. [27], [28], [7] study unimodular sequence sets with good autocorrelations. A waveform with good autocorrelation implies that it is nearly uncorrelated with its own time-shifted versions and good cross correlation implies that any transmitted waveform is nearly uncorrelated with other timeshifted transmitted waveforms. Good correlation improves the matched filter output at the interested range bin while attenuating reflections coming from other range bins. These designs however are lack of spatial constraints. There are numerous studies that only considers the distribution of spatial power. For example, in [3], the authors devise the waveform covariance matrix $\mathbf{R}$ to match the desired pattern through semidefinite quadratic programming (SQP) technique, and then a cyclic algorithm (CA) is proposed in [4] to synthesize the constant modulus waveform matrix $\mathbf{X}$ to approximate the covariance matrix $\mathbf{R}$. [29] uses same two step approach and searches BPSK signal set for a given covariance matrix. The CA approach used in [4] is also

applied to the synthesis of constant modulus transmit signals with good auto- and cross-correlation properties in [30] without considering spatial requirements. In [6], the authors have proposed a closed form covariance matrix design method to achieve the desired beampattern based on Discrete-Fourier Transform (DFT) coefficients and Toeplitz matrices for planar antenna array, and also presented a direct constant envelope waveforms design algorithm for the desired beampattern. The DFT-based technique achieves transmit beampattern match at low complexity with the trade-off of large array necessity. In [5], authors suggested a method to directly synthesize constant modulus waveform set with sample-wise constant modulus constraints. In addition to transmit beamforming, there are many practical constraints that need to be addressed. From [14], performance of any adaptive MIMO radar technique depends on cross correlation of echoes. Note that in the phased-array radar case, the probing signals at any two target locations are fully correlated/coherent and adaptive techniques are not applicable. Additionally one can force diagonal entries of the covariance matrix to be equal so that the power of transmitted signals is same which is a practical condition. Peak to Average Ratio (PAR) of a signal below a certain level is also a practical constraint. The PAR of a signal describes how the largest value of a signal compares to the average power. Signals with high PAR require higher dynamic range on ADC/DACs. Many practical systems drive power amplifiers at saturation for increased efficiency [31].

Optimization of covariance matrix $\mathbf{R}$ satisfying these additional constraints ends up with a rank $1 < \mathrm{rank}(\mathbf{R}) < M$. The two end cases represents phased array case rank 1 and omnidirectional probing rank M. Once $\mathbf{R}$ has been determined, a signal sequence $\{\mathbf{x}(n)\}$ that has $\mathbf{R}$ as its covariance matrix can be generated using various techniques. Simply setting $\mathbf{x}(n) = \mathbf{R}^{1/2}\mathbf{w}(n)$, where $\{\mathbf{w}(n)\}$ is i.i.d random vectors with zero mean and covariance matrix $\mathbf{I}$ generates accurate waveform sets for large number of snapshots. The downside of this approach is it produces non-constant envelope signal with inefficient bandwidth and unpredicted range-Doppler resolutions. Although modulus constraint can be solved with techniques proposed by [4], this brings another costly optimization to the beamforming problem. [5] proposed techniques that results in desired beampattern directly (skipping R) from constant envelope sets but leaving bandwidth and range sidelobe constaints untouched. [7]

considers only range-Doppler resolutions of the MIMO signals which results in omnidirectional probing.

We propose a new space-time coding scheme such that constructed signal set have the following features

(a) Low PAR

(b) Band-limited

(c) Low range-Doppler sidelobe

(d) Low cross-correlations between targets

(e) Generates desired beamforming

1.2 Contributions and Novelties

Our contributions are as follows:

- In Chapter 2.2.2, generalization of Woodward's ambiguity function is derived for multiple antenna/multiple waveform MIMO case. With this derivation, previous studies on beamforming designs with different constraints and studies that aim to achieve good temporal characteristics are shown to be special regions of the generalized MIMO ambiguity function. The derived function therefore leads to an optimization problem where it is possible to define interested cuts and shape the generalized ambiguity function.

- In Chapter 3.1, we propose a modified Costas coding where each chip jumps to a different phase when frequency hopping occurs as opposed to the conventional Costas codes which is based only on frequency hopping. The addition of phase terms does not degrade the good properties of Costas waveforms and they still satisfy low range sidelobe characteristics. With this coding scheme (as we call Phased-Costas waveforms) it allows us to form coherent waveforms to obtain desired beamforming in space while utilizing inherent orthogonality properties of Costas codes in time.

- In Chapter 3.2, we convert the problem to a suitable format that is solvable by ADMM in order to find the phase codes of waveforms. We set the desired beam to the related cut of the ambiguity function with additional spatial(cross) correlation and PAR constraints. We turn the resulting nonconvex objective function with nonconvex PAR constraints to a convex problem and efficiently solve it in polynomial complexity. The formulation of this problem allows us to select the power of each antenna and PAR of each waveform transmitted from the radar while keeping cross correlations of signals transmitted to targets low and satisfying desired beampattern.

1.3 The Outline of the Thesis

In Chapter 2, a brief overview of MIMO radar systems is presented. The two main structures, namely Distributed MIMO systems and Colocated MIMO systems, are investigated in terms of their benefits and differences in Chapter 2.1. The signal models for these structures are presented and several features of each system are explained. In Chapter 2.2 standard ambiguity function for SISO radars is briefly described and generalized form to the MIMO case is presented in a simplified form.

Chapter 3 sets the framework for building the Phased-Costas waveforms to satisfy requirements imposed on generalized ambiguity function derived in Chapter 2. Chapter 3.1.1 and Chapter 3.1.2 is about the frequency and phase coding of the waveforms, respectively. Chapter 3.2 is about the application of ADMM method to general problem defined in Chapter 3.1.2.

In Chapter 4.1, we present convergence performance of the proposed algorithm. We show features of the optimized waveforms in terms of its time-frequency distribution, single and multibeam performance and CDF distribution. Lastly, we present Capon and GLRT spatial spectrum of the signals under white Gaussian noise in a three target scenario as an application of the optimized waveforms.

Notation: Lowercase letters **a** denote column vectors and uppercase letters $\mathbf{A}$ denote matrices. The symbols $(\cdot)^T, (\cdot)^H, (\cdot)^C$ represents transpose, conjugate transpose and conjugate operators. The n th element of a vector **a** is written as $a(n)$. $y_n^{\tau,\nu,f}(t)$ represents the received modulated baseband signal at antenna n from a target specified with parameters delay (τ), doppler (ν) and spatial frequency (f) and $x_{nm}^{\tau,\nu,f}(t)$ represents the received signal of the target with same parameters from the n-th receive antenna due to the transmitted signal $x_m(t)$. $\otimes$ denotes Kronecker product and operator vec cascades each column in a single column.

CHAPTER 2

OVERVIEW OF MIMO RADAR

2.1 MIMO Radar

2.1.1 Distributed MIMO Radar

Distributed MIMO systems employs multiple, spatially distributed transmitters and receivers. In the context of radars, it can be defined as a system where multiple transmit waveforms reflected from targets are jointly processed at multiple receive antennas. MIMO radars has it roots from MIMO communication systems where both structures share two important property; diversity gain and spatial multiplexing [9]. Parallel to the MIMO communication systems where diversity gain obtained in the communication problem over fading channels, MIMO radars achieve diversity gain combining target returns resulting from independent illuminations of the target. The second similarity of two is the spatial multiplexing, which in MIMO communications expresses the ability to use transmit and receive antennas to set up a multidimensional space to enable uncoupled channels to grow the rate of communication. In MIMO radar case, this multidimensional space may be used to combine reflections of the target to generate a rich backscatter [9]. Distributed MIMO makes use of the spatial diversity of target RCS [10] and handles slow moving targets by making estimates from multiple directions [32]. Spatial diversity is also very effective in high resolution target localization [33].

In order to show how spatial diversity is achieved, consider the case shown in Figure 2.1 to see the spatial decorrelation of signals reflected from multiscatterers of an extended object. Assume an extended object consist of Q isotropic scatterers

each located at $X_q = (x_q, y_q)$ in the same coordinate system with M transmit antennas located at $T_k = (x_{tk}, y_{tk})$ for $k = 1 \cdots M$ and N receive antennas located at $R_l = (x_{rl}, y_{rl})$ for $l = 1 \cdots N$. Figure 2.1 shows widely separated MIMO transmit and receive antennas together with 4-point scatterers of an extended target.

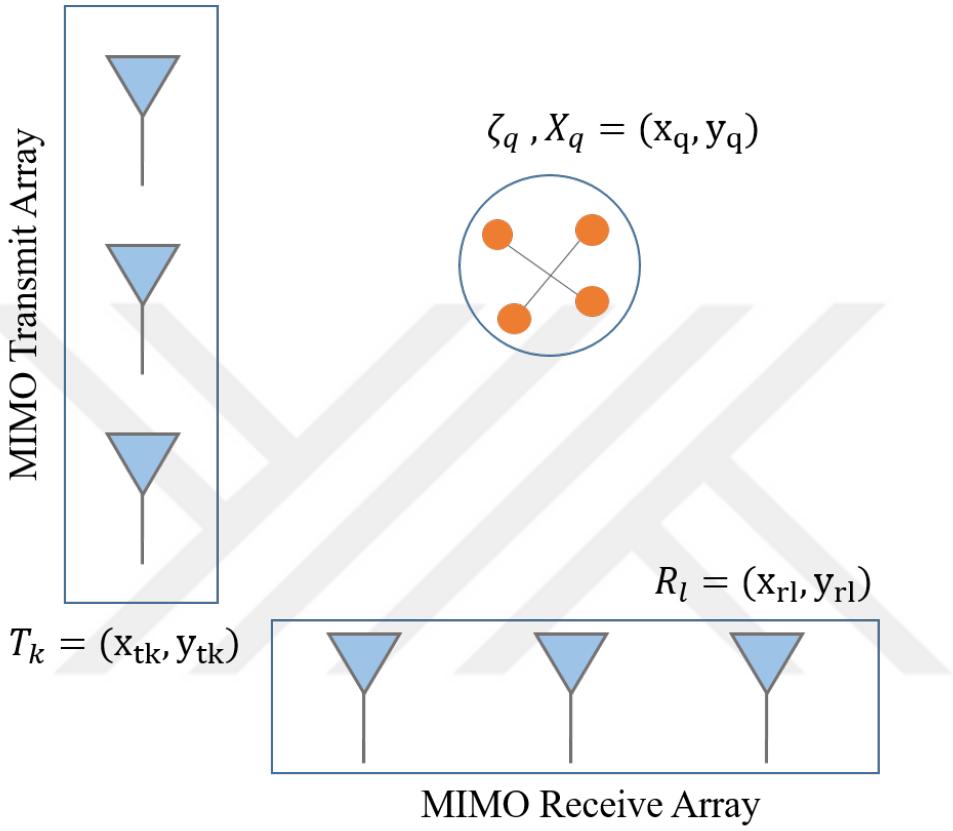

Figure 2.1: Distributed MIMO Radar with an Extended Target of 4-scatterers

To model these scatterers, it is assumed reflectivity of each scatterer is modeled by a zero mean, independent and identically distributed (i.i.d) complex random variable ζ with variance $1/Q$. Denoting $Q \times Q$ matrix $\Sigma = \text{diag}(\zeta_1, \cdots, \zeta_Q)$, the target average RCS is becomes $E[tr(\Sigma\Sigma^H)] = 1$ independent from the number of scatterers. Let $s_k(t)$ be the baseband equivalent signal transmitted from the k-th transmitter, (2.1) gives the received signal scattered by the target and collected by the l-th receiver ignoring path losses and focusing only on the effect of sensor target locations [9],

$$\begin{aligned} \boldsymbol{z}_{\ell k}^{(q)}(t) =& \sqrt{\frac{E}{M}} \zeta_q s_k \left(t - \tau_{tk}\left(X_q\right) - \tau_{r\ell}\left(X_q\right)\right) \\ & \times \exp\left(-j2\pi f_c \left[\tau_{tk}\left(X_q\right) + \tau_{r\ell}\left(X_q\right)\right]\right) \end{aligned} \tag{2.1}$$

where $\sqrt{E/M}$ is the normalization coefficient to make total energy transmitted by the radar E using unit energy signal $s_k(t)$, $\tau_{tk}\left(X_q\right) = d\left(T_k, X_q\right)/c$ is the propagation delay between k-th transmitter and q-th scatterer where $d(T_k, X_q) = \sqrt{(x_{tk} - x_q)^2 + (y_{tk} - y_q)^2}$, f_c is the carrier frequency and τ_{rl} is the delay between q-th scatterer and l-th receiver which can be found similarly as τ_{tk}.

Using the signal model given in (2.1), we can define scaling coefficient of the signal as in (2.2) which act as equivalent "channel" between transmitter k , scatterer q and receiver l.

$$h_{\ell k}^{(q)} = \zeta_q \exp\left(-j2\pi f_c \left[\tau_{tk}\left(X_q\right) + \tau_{r\ell}\left(X_q\right)\right]\right) \tag{2.2}$$

Using (2.2) in (2.1) and assuming the bandwidth of the transmitted waveforms is not enough to resolve different scatterers [9], we write (2.3) with respect to the center of scatterers denoted as X_0 and $h_{\ell k} = \sum_{q=1}^{Q} h_{\ell k}^{(q)}$ corresponds to path gains between transmitter k and receiver l.

$$z_{\ell k}(t) = \sqrt{\frac{E}{M}} h_{\ell k} s_k \left(t - \tau_{tk}\left(X_0\right) - \tau_{r\ell}\left(X_0\right)\right) \tag{2.3}$$

The matrix form $\mathbf{H}$ of the “channel" is therefore can be written as $N \times M$ matrix as expressed in [34] where $\mathbf{G} = \left[\mathrm{g}_1^T; \mathrm{g}_2^T; \ldots; \mathrm{g}_Q^T\right]$, $\mathbf{g}_q^T = [\exp[-j2\pi f_c \tau_{t1}(X_q)], \ldots, \exp[-j2\pi f_c \tau_{tM}(X_q)]$ and $\mathbf{K} = [\mathrm{k}_1, \mathrm{k}_2, \ldots, \mathrm{k}_Q]$ and $\mathbf{k}_q^T = [\exp[-j2\pi f_c \tau_{r1}(X_q)], \ldots, \exp[-j2\pi f_c \tau_{rN}(X_q)]]$

$$\mathbf{H} = \mathbf{K}\boldsymbol{\Sigma}\mathbf{G} \tag{2.4}$$

[10] shows that channel matrix can be constructed as where each element of H represents path gain of transmitter receiver pair. If at least one of the conditions in (2.5) is satisfied, then lk-th and ji-th elements of spatial matrix are uncorrelated hence spatial

decorrelation is satisfied, which actually implies that to obtain path diversity of an extended target, MIMO radar antennas should be widely separated.

$$\begin{aligned}
\frac{x_{tk}}{d\left(T_k, X_0\right)} - \frac{x_{ti}}{d\left(T_i, X_0\right)} &> \frac{\lambda}{D_x} \\
\frac{y_{tk}}{d\left(T_k, X_0\right)} - \frac{y_{ti}}{d\left(T_i, X_0\right)} &> \frac{\lambda}{D_y} \\
\frac{x_{rt}}{d\left(R_\ell, X_0\right)} - \frac{x_{rj}}{d\left(R_j, X_0\right)} &> \frac{\lambda}{D_x} \\
\frac{y_{r\ell}}{d\left(R_\ell, X_0\right)} - \frac{y_{rj}}{d\left(R_j, X_0\right)} &> \frac{\lambda}{D_y}
\end{aligned} \tag{2.5}$$

Diversity gain can be used for better target detection capability [10], [35] , improved direction finding performance [35], and better moving target detection [32]. The other benefit of distributed MIMO radar as introduced earlier is spatial multiplexing which can be interpreted as the number of targets that can be handled simultaneously. The rank of channel matrix $\mathbf{H}$ is bounded by the ranks of $\mathbf{K}$ which is N for sufficiently separated receive antennas, $\mathbf{G}$ which is M for sufficiently separated transmit antennas, and $\mathbf{\Sigma}$ which is Q for point targets [9]. Therefore if $Q \leq \min\left(M, N\right)$ estimate of the number of targets can be found using singular value decomposition of $\mathbf{H}$.

2.1.2 Colocated MIMO Radar

Colocated MIMO radar as its name suggests is the structure where transmit and receive elements are closely spaced similar to phased-array radars. The difference, however, unlike phased array case where it sends only a complex multiple of the same signal (also called weights), it can send signals that may be correlated or uncorrelated with each other depending on the application. This diversity enables superiority in many aspects, including target identifiability, parameter estimation quality and beampattern design.

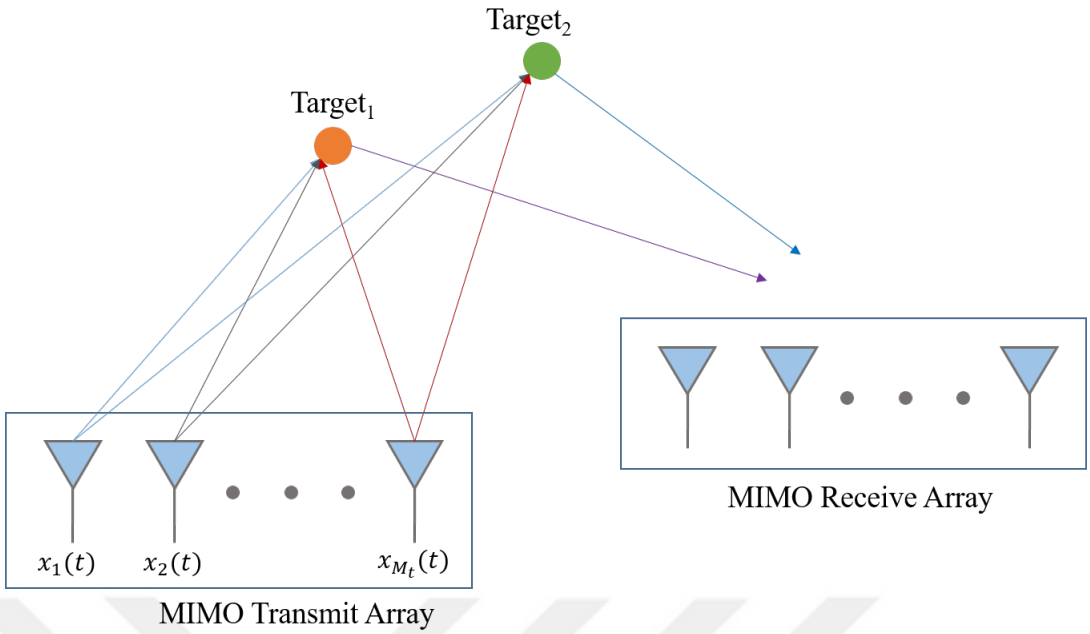

Figure 2.2: Collocated MIMO Structure with Uncorrelated Waveforms

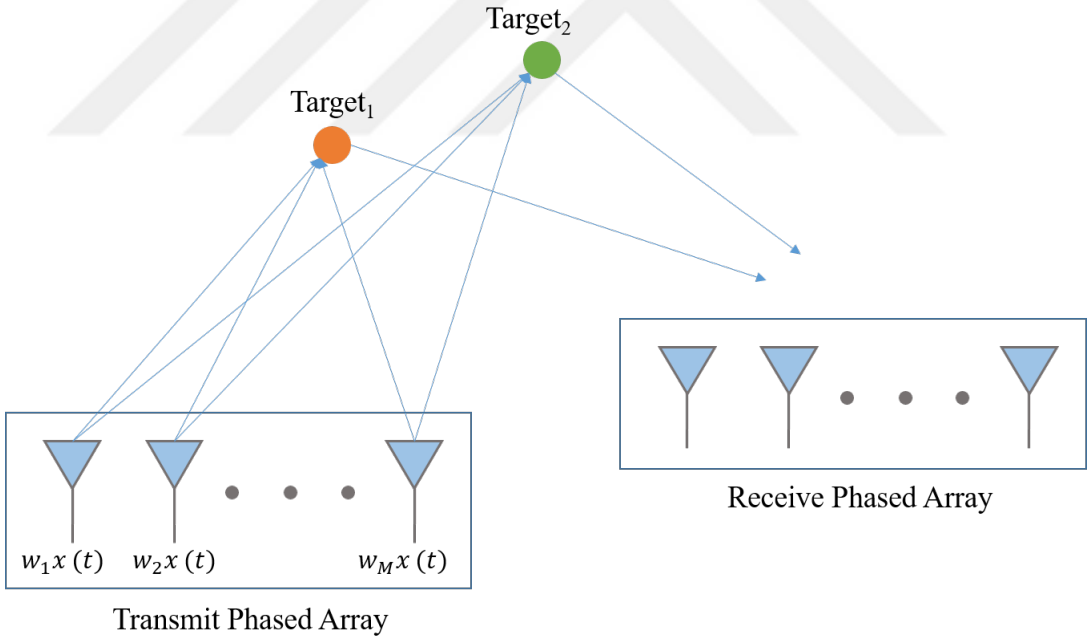

Figure 2.3: Phased Array Array Radar with Weighted Waveforms

- Identifiability

  Parameter identifiability is most striking benefit of the colocated MIMO systems. It shows the maximum number of targets that can be uniquely identified by the radar. Compared to phased array counterpart, the identifiable target size can be increased up to M_t times higher depending on efficient antenna placement by adjusting the virtual array and selecting independent waveform set [1]. To formulate the identifiability problem, consider a collocated MIMO system with M_t transmit antennas and M_r receive antennas. Let $x_m(n)$ denote discrete time baseband signal transmitted by the m-th antenna.

$$\sum_{m=1}^{M_t} e^{-j2\pi f_0 \tau_m(\theta)} x_m(n) \triangleq \mathbf{a}_T^H(\theta)\mathbf{x}(n), \quad n = 1, \ldots, N_s \tag{2.6}$$

where f_0 is the carrier frequency of the radar, $\tau_m(\theta)$ is the propagation time delay between m-th transmit antenna and the target. The signal vector and transmit steering vector are defined as

$$\mathbf{x}(n) = [x_1(n)\, x_2(n)\, \ldots\, x_{M_t}(n)]^T \tag{2.7}$$

$$\mathbf{a}_T(\theta) = \left[e^{j2\pi f_0 \tau_1(\theta)}\, e^{j2\pi f_0 \tau_2(\theta)}\, \ldots\, e^{j2\pi f_0 \tau_{M_t}(\theta)}\right]^T \tag{2.8}$$

Similarly receive signal can be formulated as

$$\mathbf{y}(n) = \sum_{k=1}^{K} \beta_k \mathbf{a}_R^C(\theta_k)\, \mathbf{a}_T^H(\theta_k)\, \mathbf{x}(n) + \boldsymbol{\epsilon}(n), \quad n = 1, \cdots, N_s \tag{2.9}$$

where $\tilde{\tau}_m(\theta)$ is the time delay between target and m-th receive antenna and

$$\mathbf{y}(n) = [y_1(n)\, y_2(n)\, \ldots\, y_{M_r}(n)]^T \tag{2.10}$$

$$\mathbf{a}_R(\theta) = \left[e^{j2\pi f_0 \tilde{\tau}_1(\theta)} e^{j2\pi f_0 \tilde{\tau}_2(\theta)} \ldots e^{j2\pi f_0 \tilde{\tau}_{M_r}(\theta)}\right]^T \tag{2.11}$$

[13] shows that as the number of snapshots or signal-to-interference-plus-noise ratio (SINR) goes to infinity (assuming interfence-plus-noise term is uncorrelated with transmit signal), the effect of noise or interference can be eliminated hence identifiability is inherent feature of the array that is independent of noise.

In (2.12), β_k and θ_k for $k = 1 \cdots K$ are the target parameters to be found from received vector $\mathbf{y}(n)$. "Identifiability equation" is given in [13] as

$$\sum_{k=1}^{K} \beta_k^* \mathbf{a}_R^C(\theta_k^*) \mathbf{a}_T^H(\theta_k^*) \mathbf{x}(n) = \sum_{k=1}^{K} \beta_k \mathbf{a}_R^C(\theta_k) \mathbf{a}_T^H(\theta_k) \mathbf{x}(n),\ n = 1, \cdots, N \tag{2.12}$$

In order to identify each target, it requires $\beta_k^* = \beta_k$ and $\theta_k^* = \theta_k^*$ for all $k = 1 \cdots K$. If each transmitted signal $x_m(n)$ is independent from each other, that is $\mathrm{rank}\{[\mathbf{x}(1) \quad \cdots \quad \mathbf{x}(N)]\} = M_t$, (2.12) can be rewritten as [13]

$$\sum_{k=1}^{K} \beta_k^* \mathbf{a}_R^C(\theta_k^*) \mathbf{a}_T^H(\theta_k^*) = \sum_{k=1}^{K} \beta_k \mathbf{a}_R^C(\theta_k) \mathbf{a}_T^H(\theta_k) \tag{2.13}$$

or

$$\mathbf{A}^* \boldsymbol{\beta}^* = \mathbf{A} \boldsymbol{\beta} \tag{2.14}$$

where

$$\boldsymbol{\beta} = [\beta_1 \ \cdots \ \beta_K]^T \tag{2.15}$$

$$\boldsymbol{\beta}^* = [\beta_1^* \ \cdots \ \beta_K^*]^T \tag{2.16}$$

$$\mathbf{A} = \left[\mathbf{a}_T^C(\theta_1) \otimes \mathbf{a}_R^C(\theta_1) \quad \cdots \quad \mathbf{a}_T^C(\theta_K) \otimes \mathbf{a}_R^C(\theta_K)\right] \tag{2.17}$$

$$\mathbf{A}^* = \left[\mathbf{a}_T^C(\theta_1^*) \otimes \mathbf{a}_R^C(\theta_1^*) \quad \cdots \quad \mathbf{a}_T^C(\theta_K^*) \otimes \mathbf{a}_R^C(\theta_K^*)\right] \tag{2.18}$$

The number of identifiable target parameters is therefore depends on the number of distinct elements in the columns of $\mathbf{A}$. In comparison with phase array radar, MIMO radar can identify twice as many targets in the worst case [1], which is from identifiability perspective is when a filled uniform linear array (ULA) is used for both transmit and receive (i.e $M_t = M_r$), $\mathbf{a}_R(\theta) = \mathbf{a}_T(\theta)$ and $\mathbf{A}$ has only $2M - 1$ distinct elements although it can increase up to M^2. A nonuniform but still linear array can increase up to $(M^2 + M)/2$ independent elements, and the most general case where $M_t \neq M_r$ if arranged as ULA, distinct element size becomes $M_t + M_r + 1$. In the case of a filled M_r receive element but sparse M_t transmit elements with $M_r/2$ interelement spacing, virtual aperture of the system reaches the maximum $M_t M_r$ length, that is M_t times

larger than the real receive element M_r. In summary, the bounds for collocated MIMO and phased-array comparison in terms of target identifiability depending on the array geometry and the number of antennas shared between transmit and receive elements can be expressed as [1]

$$K_{\max_{MIMO}} \in \left[\frac{M_t + M_r - 2}{2}, \frac{M_t M_r + 1}{2}\right) \tag{2.19}$$

$$K_{\max_{Phased}} = \left\lceil \frac{M_r - 1}{2} \right\rceil \tag{2.20}$$

For numeric demonstration, [13] shows Cramer-Rao-Bound(CRB) for θ_1 of both MIMO Radar and Phased-Array Radar for the number of targets using Slepian-Bangs formula. It shows that for uniform linear array of size $M = 10$ with $\lambda/2$ spacing , identifiable target of MIMO Radar is almost constant while Phased-Array goes unbounded after K = 4. This result agrees with the formulations (2.19)-(2.20) proposed by [1].

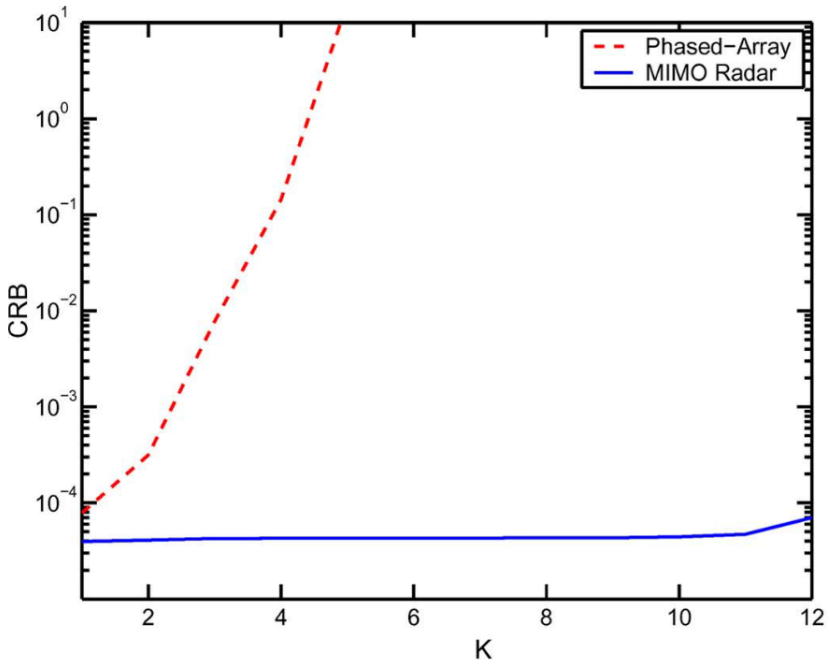

Figure 2.4: CRB of θ_1 Collocated MIMO vs Phased Array with respect to Target Number K [1]

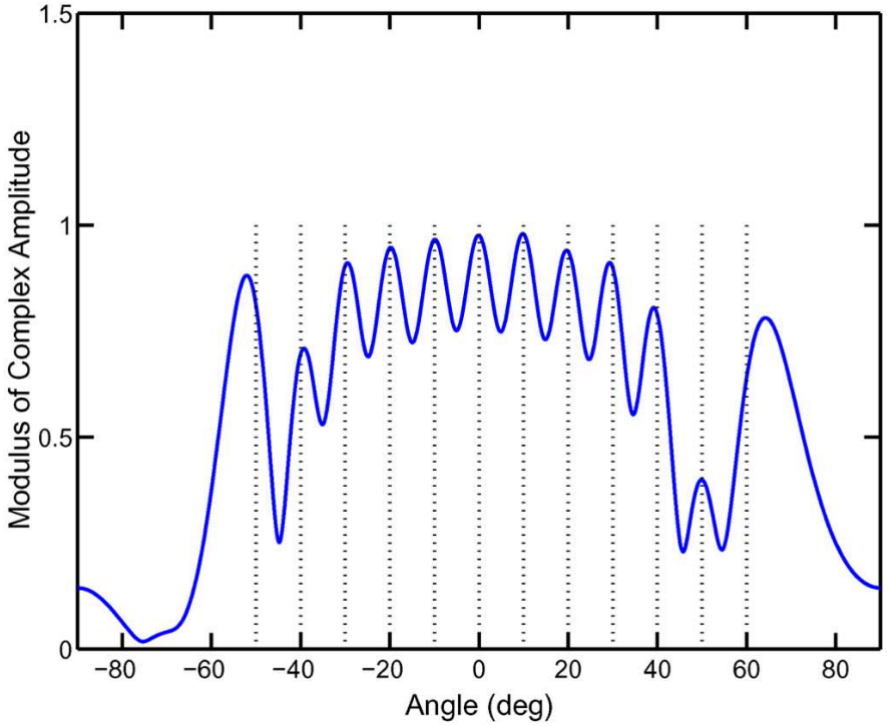

Figure 2.5: Least squares spatial spectrum for $K = 12$ using ULA with $M = 10$ antennas and 0.5-wavelength interelement spacing [1]

- Parameter Estimation

  As shown recently in [1], direct application of adaptive techniques is possible for MIMO radars. To show this, let $\tilde{\mathbf{A}}$ be defined as

$$\tilde{\mathbf{A}} = [\beta_1^* \mathbf{a}_T(\theta_1) \ \beta_2^* \mathbf{a}_T(\theta_2) \ \cdots \ \beta_K^* \mathbf{a}_T(\theta_K)] \tag{2.21}$$

  then the sample covariance matrix of the reflected waveforms from K different targets becomes $\tilde{\mathbf{A}}^H \mathbf{R}_x \tilde{\mathbf{A}}$ where $\mathbf{R}_x = \mathbf{I}$ if orthogonal signals are used and number of snapshots is much greater than M_t (which is a practical case). Then $\tilde{\mathbf{A}}^H \mathbf{R}_x \tilde{\mathbf{A}}$ has full rank if columns of $\tilde{\mathbf{A}}$ are linearly independent which requires $K < M_t$. This property allows direct application of adaptive techniques for target localization [1].

- Beampattern Design

  The signal set transmitted by a MIMO transmit antennas can be designed to focus on desired spatial locations and also to minimize cross correlations of the signals reflected from various angular sectors. [3], [29] provides the pioneering work that shows the necessary formulation and constraints for the transmit beampattern problem and the requirements where phased arrays fail. Using the diversity of transmitting correlated/uncorrelated waveforms, it is possible to cohere signals in desired directions resulting in desired beampatterns. Using the signal set in (2.7), the power of the transmitted signals at an angle θ is expressed as

$$P(\theta) = \mathbf{a}_T^H(\theta)\mathbf{R}\mathbf{a}_T(\theta) \tag{2.22}$$

  where $\mathbf{R} = E\left\{\mathbf{x}(n)\mathbf{x}^H(n)\right\}$ denotes covariance matrix of $\mathbf{x}(n)$. $P(\theta)$ is also called as transmit beampattern and further discussions can be found on [29]. Depending on the covariance matrix $\mathbf{R}$ many possibilities exist; if for example signals are fully correlated as in the case of phased array radars where each signals is only a complex multiple of each other, rank($\mathbf{R}$) reduces to one, whereas it becomes full rank if all waveforms are uncorrelated. In order to explore its effect on beampattern, we show a highly structured correlation matrix explored in [29], to see the extreme cases from perfect coherence to fully uncorrelated case. Let $\mathbf{R}$ be an $M_t \times M_t$ Toeplitz matrix describing the autocorrelation of a first order Markov process, parameterized by ρ, $0 \leq \rho \leq 1$.

$$\mathbf{R} = \begin{bmatrix} 1 & \rho & \rho^2 & \rho^3 & \cdots & \rho^{M_t-1} \\ \rho & 1 & \rho & \rho^2 & & \vdots \\ \rho^2 & \rho & 1 & \rho & & \\ \rho^3 & \rho^2 & \rho & 1 & \ddots & \\ \vdots & & & \ddots & \ddots & \rho \\ \rho^{M_t-1} & \cdots & & & \rho & 1 \end{bmatrix}$$

  Notice that $\rho = 0$ represents fully uncorrelated case (i.e $\mathbf{R} = \mathbf{I}$ and $\rho = 1$ represents perfect coherent case (i.e $\mathbf{R} = \mathbf{1}\mathbf{1}^T$). Figure shows the resulting beampatterns for $0 \leq \rho \leq 1$. Omnidirectional pattern is created when all the signals are uncorrelated and focused beam corresponds to fully coherent

waveform set.

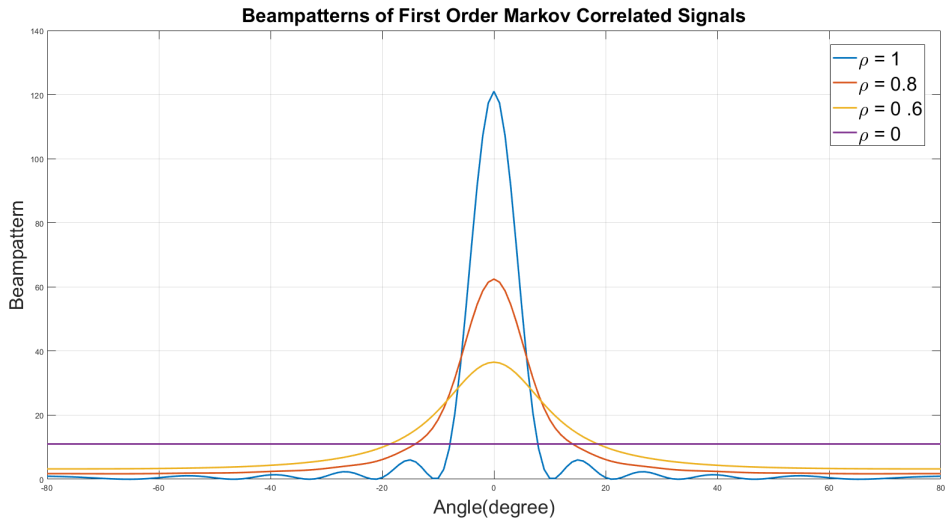

Figure 2.6: Beampatterns of First-Order Markov Correlated Signals

This Toeplitz structure is only among many other possibilities $\mathbf{R}$ can have. Designing beamformers with different constraints leads to other matrices. Two general requirement in the optimization of beamformer is to maximize power at a number of given target location and minimize the cross correlation between targets ($\mathbf{a}_T^H(\theta_i)\mathbf{R}\mathbf{a}_T(\theta_j)$ for $i, j = 1 \cdots K, i \neq j$) so that adaptive techniques are applicable. The latter requirement is justified by related works [14], note that in phased-array radars transmitted signals at any two locations θ_i and θ_j are fully correlated and it is not possible to use adaptive techniques.

Covariance matrix based optimization can be solved for different criteria. For example without having any prior information about target sectors, one can design maximum power for unknown targets as formulated by [3]

$$\sum_{k=1}^{K} \mathbf{a}_T^H(\theta_k)\,\mathbf{R}\mathbf{a}_T(\theta_k) \triangleq \mathrm{tr}(\mathbf{RB})$$

where

$$\mathbf{B} = \sum_{k=1}^{K} \mathbf{a}_T(\theta_k)\,\mathbf{a}_T^H(\theta_k)$$

Since there is no crude estimates of targets ($k = 1 \cdots K$), it implies that $\mathbf{B}$ is not available apriori. Therefore optimization problem becomes [3]

$$\begin{aligned} &\max_{\mathbf{R}} \min_{\mathbf{B}} \operatorname{tr}(\mathbf{RB}) \\ &\textit{s.t}\ \ R_{mm} = \frac{c}{M} \text{ for } m = 1 \cdots M \\ &\qquad \mathbf{R} \geq 0 \\ &\qquad \mathbf{B} \geq 0 \text{ and } \lambda_p(\mathbf{B}) \geq \epsilon \text{ for some } \epsilon > 0, p \in [1, M] \end{aligned} \tag{2.23}$$

This min max problem tries to maximize beampattern in the worst case when $\mathbf{B}$ makes $\operatorname{tr}(\mathbf{RB})$ minimum. The constraints of $\mathbf{R}$ is to set elemental powers of each antenna and to make covariance matrix positive semidefinite. The constraint for the eigenvalues of B is to avoid the trivial solution of $\mathbf{B} = 0$. This elemental power constraint is relaxed to a total power constraint such that $\operatorname{tr}(\mathbf{R}) = c$, the solution to the problem is given by [36] as

$$\mathbf{R} = \frac{c}{M}\mathbf{I}$$

This solution corresponds to the fully uncorrelated signal set since $\mathbf{R}$ is full rank, and intuitively tells that if there is no prior information for the targets, optimum beampattern should be spatially white corresponding to the case $\rho = 0$ in Figure 2.6.

If prior knowledge on $\hat{\mathbf{B}}$ of $\mathbf{B}$ exist, then inner term is omitted and optimization problem becomes [3]

$$\begin{aligned} &\max_{\mathbf{R}} \operatorname{tr}(\mathbf{RB}) \\ &\textit{s.t}\ \ \operatorname{tr}(\mathbf{R}) = c \\ &\qquad \mathbf{R} \geq 0 \end{aligned} \tag{2.24}$$

The solution to this problem is given by [3]

$$\mathbf{R} = c\mathbf{u}\mathbf{u}^H \tag{2.25}$$

where $\mathbf{u}$ is the unit norm eigenvector associated with the largest eigenvalue of $\hat{\mathbf{B}}$. The solution (2.26) for single target case reduces to delay and sum beamformer.

$$\mathbf{R} = c\frac{\mathbf{a}_T(\hat{\theta})\mathbf{a}_T^H(\hat{\theta})}{\|\mathbf{a}_T(\hat{\theta})\|^2} \tag{2.26}$$

However, (2.25) has significant disadvantages. Although we focus the energy to the collection of targets, how it is distributed individually is not controlled.

Also cross correlation requirement between targets expressed in (2.27) is not included in this method.

$$\Gamma = \mathbf{a}_T^H(\theta_i)\mathbf{R}\mathbf{a}_T(\theta_j) \quad \text{for} \quad i,j = 1 \cdots K, i \neq j \tag{2.27}$$

The third disadvantage is that, after having found covariance matrix $\mathbf{R}$ we still need to generate signal set satisfying this covariance requirement. The most straightforward solution to this is setting $\mathbf{x}(n) = \mathbf{R}^{1/2}\mathbf{w}(n)$, where $\mathbf{w}(n)$ is independent and identically distributed zero mean , unit variance random vector. However signals generated this way do not have practical waveform constraints such as constant modulus or low peak to average ratio. In addition, the bandwidth of the signal is not constrained and spectral shaping of the waveforms should be considered. Methods proposed by various studies [3], [4], [29] involve another costly optimization for generating waveforms satisyfying $\mathbf{R}$ with additional constraints and overall problem becomes two-step optimization, finding optimum covariance matrix and finding proper waveform set.

2.2 Generalized Ambiguity Function

2.2.1 Conventional Ambiguity Function

Conventional ambiguity function, also known as Woodwards ambiguity function, is the matched filter output in the receiver when a delay mismatch τ and Doppler mismatch v occurs on the returning signal as defined in (2.28) where $x(t)$ is the baseband equivalent of the transmitted signal.

$$\chi(\tau,\nu) \triangleq \int_{-\infty}^{\infty} x(t)x^*(t+\tau)e^{j2\pi\nu t}dt \tag{2.28}$$

The value $\chi(0,0)$ represents when there is no mismatch. A sharp peak around $\chi(0,0)$ is desired for a good radar waveform in order to have good resolution in range(delay) and Doppler. In other words, ideally we expect a 2-dimentional Dirac delta function that has a peak at $\chi(0,0)$ and zero everywhere else.

$$\chi(\tau,f) = \delta(\tau)\delta(f) \tag{2.29}$$

However ambiguity function of this kind is impossible with practical finite duration and bandlimited signals. Figure 2.7 - Figure 2.10 shows two examples; one with a simple rectangular pulse and the other with LFM modulated pulse. Both pulses have duration of 50 μs with LFM having an upsweep of 100 kHz centered at 0 Hz. Notice that LFM has better range resolution with the increase in bandwidth in the signal. Also notice that Doppler resolution is same since a single pulse is not enough to resolve Doppler shift as will be derived in the next section.

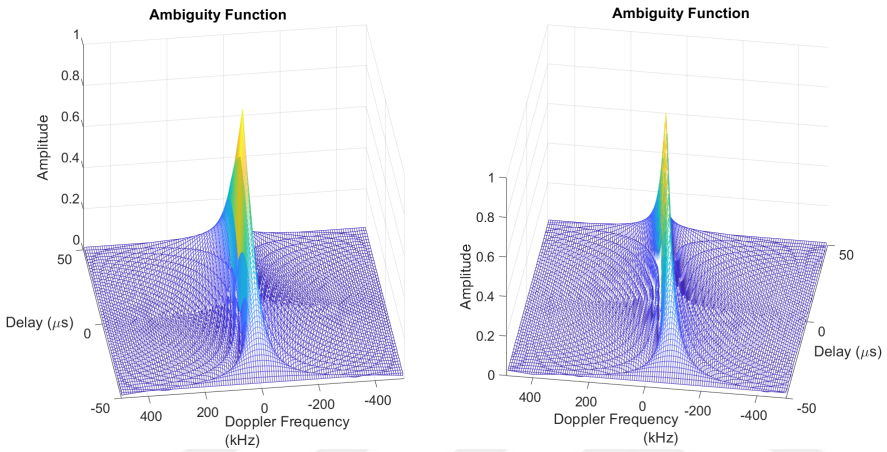

Figure 2.7: 3D Ambiguity Plot of Simple Pulse and LFM Coded Pulse

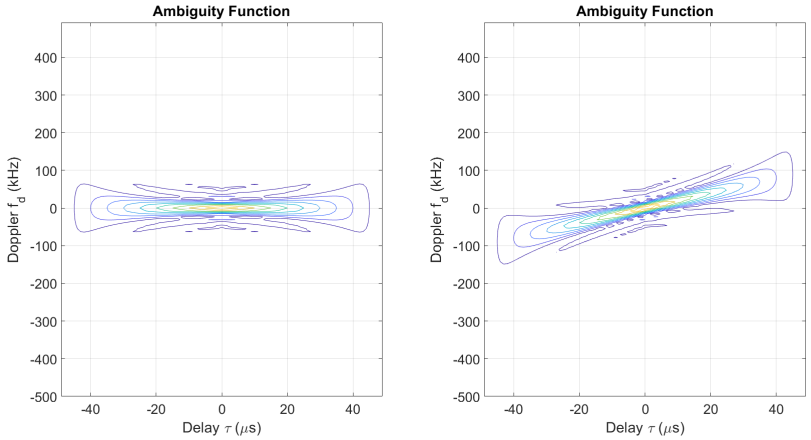

Figure 2.8: 2D Contour Plot of Simple Pulse and LFM Coded Pulse

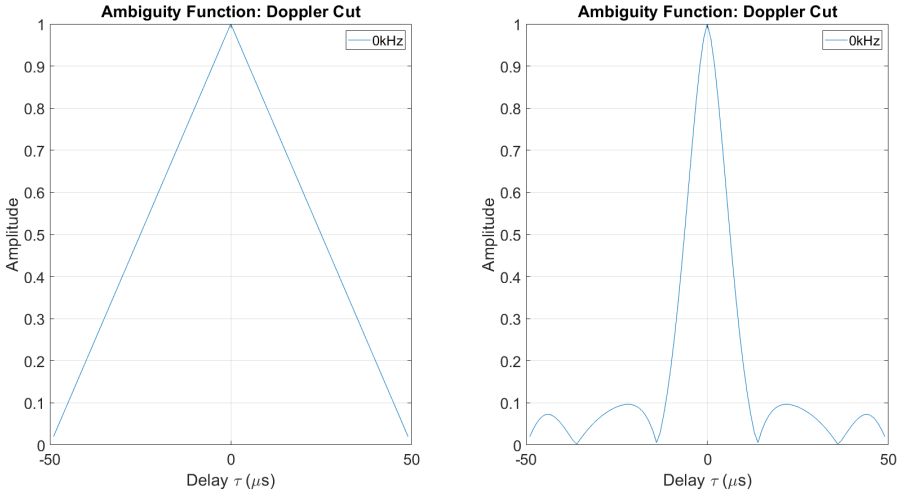

Figure 2.9: $f_d = 0\ kHz$ Doppler Cut for Simple Pulse and LFM Coded Pulse

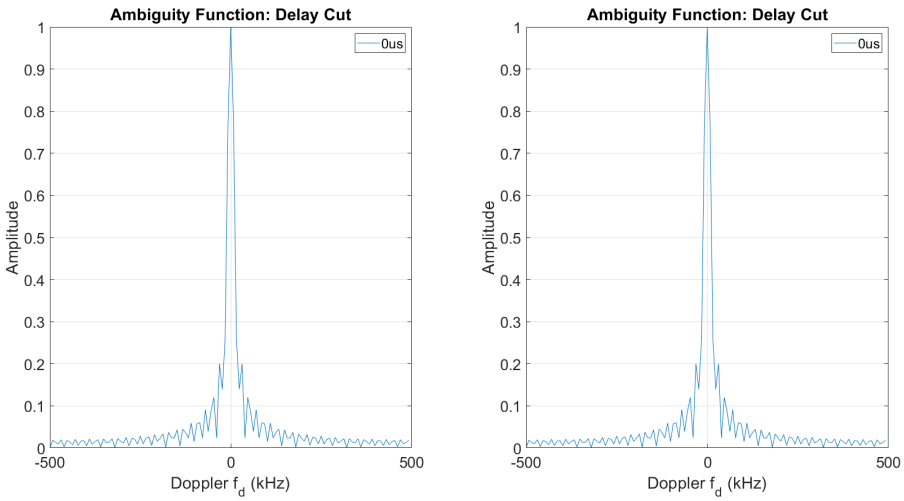

Figure 2.10: $\tau = 0\ \mu s$ Delay Cut for Simple Pulse and LFM Coded Pulse

2.2.2 MIMO Ambiguity Function

In MIMO radar case, there will be multiple independent signals emitting from the antennas instead of a single waveform $x(t)$ used in (2.28). Also in addition to single antenna case, MIMO structure also implements spatial filtering. Therefore ambiguity function definition needs to be generalized for multiple signal/multiple antenna case. In conventional form ambiguity function shows the resolution properties of the waveforms in delay and Doppler, for the MIMO generalized case spatial resolution should also be included in the definition. [7], [37] and [38] did a very detailed extension of (2.28) to MIMO case, however, expressions are not very suitable for multiple constraint optimization. In this paper, a simple form for MIMO radar ambiguity function is obtained leading to optimum solution of beampatterns with PAR constraints.

A target with a specific range, velocity and angle can be defined with three corresponding parameters for the signal model. Let τ be the delay corresponding to the range of the target, v is the Doppler shift due to the velocity and f is the *normalized spatial frequency* of the target defined as

$$f \triangleq \frac{d_R}{\lambda} \sin\theta \tag{2.30}$$

where the spatial location of the target $\theta \in [-90, 90]$ is defined with respect to the boresight of colocated ULA with transmitting and receiving antennas placed as in Figure 2.11. For the antenna spacing of $d_T = d_R = \lambda/2$, spatial frequency becomes $f \in [-0.5, 0.5]$. Figure 2.11 shows detailed structure where MIMO matched filtering in range-doppler-angle is performed. With this structure, we generalize the matched filtering concept such that received signal from a target with parameters (τ, v, f) is compared to the received signal that would be observed from a reference with parameters (τ', v', f') which is expected to be matched if target is very close to the reference.

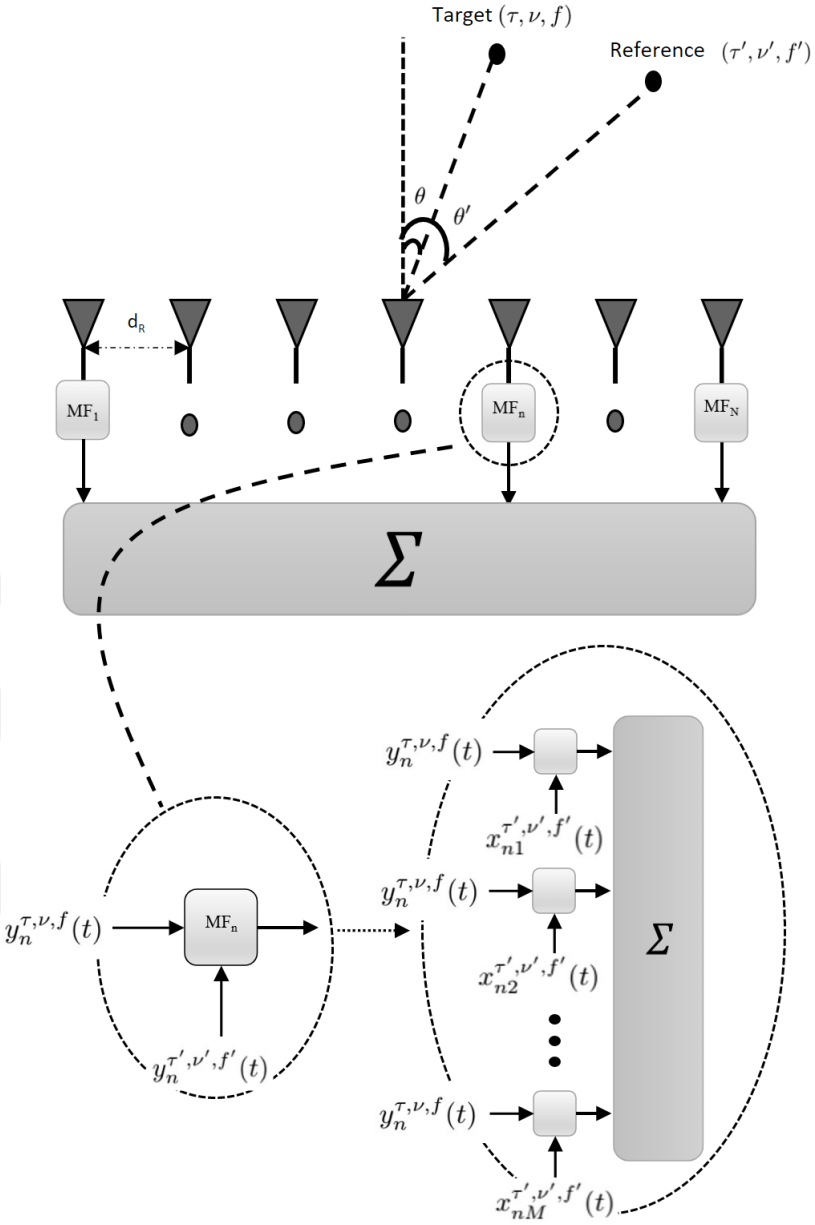

Figure 2.11: MIMO Matched Filtering of received signals where $y_n^{\tau,\nu,f}(t)$ is the received signal from the n-th antenna due to the Target (τ, v, f), $x_{nm}^{\tau',\nu',f'}(t)$ is the reflected signal off of the Reference (τ', v', f') received from the n-th antenna due to transmitted signal $x_m(t)$ from the m-th antenna.

Let $m = 0, 1, \ldots, M-1$ where M is the number of transmit antennas and $n = 0, 1, \ldots, N-1$ where N is the number of receive antennas. The demodulated target response in the n-th antenna can be written as

$$y_n^{\tau,\nu,f}(t) = \sum_{m=0}^{M-1} \xi_{mn} x_m(t-\tau) e^{j2\pi\nu t} e^{j2\pi f(m+n)} \tag{2.31}$$

where $x_m(t)$ is the radar waveform transmitted from the m-th antenna and ξ_{mn} is the complex reflection coefficient for the m-th transmit and n-th receive channels. In this thesis, we will consider the narrowband assumption and take ξ_{mn} as a unit scalar term for all the channels, similar to [7], [37] and [38]. If the receiver tries to capture this target with a matched filter with the assumed reference parameters (τ', v', f') then the matched filter output becomes [7]:

$$MF_{out} = \sum_{n=0}^{N-1} MF_n \tag{2.32}$$

$$MF_n = \int_{-\infty}^{\infty} y_n^{\tau,\nu,f}(t) \cdot \left(y_n^{\tau',\nu',f'}\right)^* (t) dt \tag{2.33}$$

$$\begin{aligned} MF_{out} = & \left(\sum_{n=0}^{N-1} e^{j2\pi(f-f')n} \right) \\ & \left(\sum_{m=0}^{M-1} \sum_{m'=0}^{M-1} \left(\int_{-\infty}^{\infty} x_m(t-\tau) x_{m'}^*(t-\tau') e^{j2\pi(\nu-\nu')t} dt \right) \right. \\ & \left. e^{j2\pi(fm-f'm')} \right) \end{aligned} \tag{2.34}$$

A careful inspection of (2.34) reveals that it can be written in terms of transmit $(\mathbf{a}_T^H)$ and receive steering vectors $(\mathbf{a}_R^H)$ as

$$MF_{out} = \left(\mathbf{a}_R^H(f)\mathbf{a}_R(f')\right)\left(\mathbf{a}_T^H(f)\mathbf{X}\mathbf{a}_T(f')\right) \tag{2.35}$$

where $\mathbf{X}$ is defined as (2.36) with time lag and Doppler shift redefined as $\tau = \tau - \tau'$, $\nu = \nu - \nu'$.

$$\mathbf{X}(\tau, v) = \begin{bmatrix} \chi_{1,1}(\tau, v) & \chi_{1,2}(\tau, v) & \ldots & \chi_{1,M}(\tau, v) \\ \vdots & \ddots & & \\ \chi_{M,1}(\tau, v) & & & \chi_{M,M}(\tau, v) \end{bmatrix} \tag{2.36}$$

$$\chi_{m,m'}(\tau,\nu) \triangleq \int_{-\infty}^{\infty} x_m(t) x_{m'}^*(t+\tau) e^{j2\pi\nu t} dt \tag{2.37}$$

First part of the equation (2.35) represents spatial processing at the receiver and it is not affected by the waveform set $\{x_m(t)\}$. Second part represents spatial, Doppler and range resolution of the system. Therefore, MIMO radar ambiguity function can be written as

$$\chi\left(\tau, v, f, f'\right) = \mathbf{a}_T^H(f)\mathbf{X}\ \mathbf{a}_T\left(f'\right) \tag{2.38}$$

Note that MIMO radar ambiguity function $\chi\left(\tau, v, f, f'\right)$ can not be written as a function of difference $f - f'$ as in delay (τ) or Doppler (v) because of the inseperability of $fm - f'm'$. One simplification to (2.38) is that since practical pulse durations are very short for moving targets, Doppler shift within the pulse (with duration T_x) is almost negligible (i.e., $T_x v \approx 0$). In pulsed radars, Doppler resolution can be improved by sending multiple pulses [39] and coherent processing interval of the pulses becomes decisive parameter. Therefore, (2.37) can be simplified as

$$r_{m,m'}(\tau) \triangleq \int_{-\infty}^{\infty} x_m(t) x_{m'}^*(t+\tau) dt \quad \text{for} \quad m, m' = 0, 1, \ldots M \tag{2.39}$$

and Doppler shift omitted version of $\mathbf{X}$ becomes

$$\mathbf{R}(\tau) = \begin{bmatrix} r_{1,1}(\tau) & r_{1,2}(\tau) & \ldots & r_{1,M}(\tau) \\ \vdots & \ddots & & \\ r_{M,1}(\tau) & & & r_{M,M}(\tau) \end{bmatrix} \tag{2.40}$$

Ambiguity function in (2.38) can be written in terms of the transmit steering vector and the correlation matrix given in (2.40). By expressing f and f', in terms of θ and θ' using (2.30), ambiguity function is expressed as

$$\Gamma\left(\tau, \theta, \theta'\right) = \mathbf{a}_T^H(\theta)\mathbf{R}(\tau)\mathbf{a}_T\left(\theta'\right) \tag{2.41}$$

Expression derived in (2.41) is a function of three parameters (τ, θ, θ'). Equation (2.27) corresponds to evaluating (2.41) at point $\tau = 0$, $\theta = \theta_1$, $\theta' = \theta_2$ and (2.22) corresponds to a specific cut of (2.41) where $\tau = 0$ and $\theta = \theta'$. (2.41) gives a large flexibility to obtain sharp ambiguity function at $\theta = \theta'$ while suppressing the cross terms for $\theta \neq \theta'$ and time sidelobes for $\tau \neq 0$. In some of the previous studies,

beamforming is not considered, (resulting in omnidirectional transmit beamforming) while τ is optimized [28], [7]. On the contrary, [3] and [5] optimize (2.27) and (2.22) without considering the sidelobes due to $\tau \neq 0$. Different from the previous studies, we present a new approach to optimize (2.41) in order to satisfy constraints both in spatial domain, (θ, θ'), and time domain, (τ). In addition, we impose PAR constraints to obtain robust beamformer designs for nonlinear amplifier structures.

Optimizing (2.41) in spatial and time domain together with additional constraints is a complex task. In order to manage this problem and obtain optimum solutions, we choose to minimize the sidelobes for different delay terms, τ, by using some special waveforms which inherently have low correlations. In the following section, Phased-Costas waveforms will be presented for this purpose.

CHAPTER 3

PHASED-COSTAS CODING OF MIMO RADAR WAVEFORMS

3.1 Problem Formulation

Each requirement itemized in Chapter 1.1, corresponds to a constraint on (2.41). For minimization of Γ along undesirable regions (c, d) and focusing ambiguity function along the region of interest (e) while satisfting the practical waveform constaints (a,b), we choose to fit waveforms in a framework as in (3.1) - (3.6) such that each generated pulse is frequency coded in time and phase coded in space. Let $x_{m_k}(t)$ be the k-th subpulse of m-th signal transmitted from the M element ULA MIMO radar. We can express the space-time coded signal set as

$$x_m(t) = \sum_{k=1}^{K} \beta_{m_k} x_{m_k} \left[t - (k-1)t_{\mathrm{b}}\right] \tag{3.1}$$

$$x_{m_k}(t) = \begin{cases} \exp\left(j2\pi f_k t + \phi_{m_k}\right), & 0 \leq t \leq t_{\mathrm{b}} \\ 0 & \text{elsewhere} \end{cases} \tag{3.2}$$

$$\mathbf{p}_k = [\phi_{1_k}, \phi_{2_k}, \ldots, \phi_{m_k}, \ldots, \phi_{M_k}] \tag{3.3}$$

$$\mathbf{P} = [\mathbf{p}_1; \ldots; \mathbf{p}_k; \ldots, \mathbf{p}_K]_{K \times M} \tag{3.4}$$

$$\mathbf{C} = \mathbf{1}_{1 \times M} \otimes [c_1, c_2, \ldots, c_K]^T \tag{3.5}$$

$$\tilde{f}_k = \frac{c_k}{t_b} \tag{3.6}$$

where $\mathbf{p}_k$ is the phase code of the M element array of the k-th subpulses to satisfy (d,e) and $\mathbf{C}$ is the frequency code to satisfy (b,c). The framework proposed satisfies constant envelope signal condition (a) with β_{m_k} fixed, or satisfies low PAR condition by keeping it within an interval. Figure 3.1 shows the resulting space time coded signal set for an array of size M. Each chip implements phase coding $\mathbf{p_k}$ sequentially up to the K-th chip.

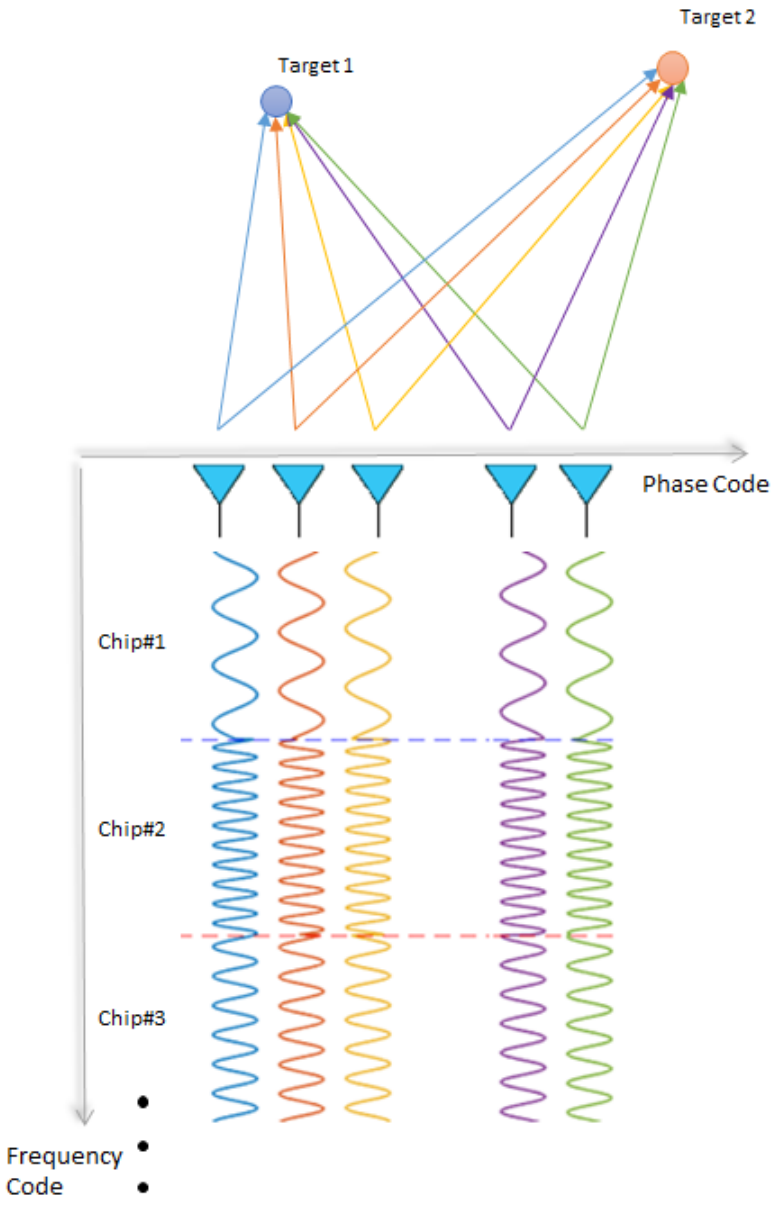

Figure 3.1: Space-Time Coded Waveform

The most general optimization problem is

$$\begin{aligned} \min_{\mathbf{C},\mathbf{P}} \quad & f(\mathbf{C};\mathbf{P}) \\ \text{subject to} \quad & \Gamma(0,\theta,\theta) = D(\theta) \end{aligned} \tag{3.7}$$

where

$$f(\mathbf{C};\mathbf{P}) \triangleq \int_{-\infty}^{\infty}\int_{-\pi/2}^{\pi/2}\int_{-\pi/2}^{\pi/2} \left|\Gamma\left(\tau,\theta,\theta'\right)\right|^2 d\theta d\theta' d\tau \tag{3.8}$$

where squared norm of the generalized ambiguity function $\left|\Gamma\left(\tau,\theta,\theta'\right)\right|^2$ implicitly depends on the frequency code $\mathbf{C}$ and phase code $\mathbf{P}$ through the waveforms. Similar to the conventional ambiguity function requirements, ideally it is desirable to place impulse-like function on desired spatial locations and supressing everywhere else. This minimization problem in (3.7) can be divided into multiple cases.

- *Case (1)* : $\tau \neq 0$, for all $\theta, \theta' \in [-\pi/2, \pi/2]$ minimize $|\Gamma(\tau,\theta,\theta')|^2$
  This case represents the range sidelobes for the signals transmitted to the different range bins of any angle. It corresponds to minimizing the ambiguity function for all nonzero time lags from all angles. This requirement aims to reduce range sidelobes sharply after $\tau = 0$ cut.

- *Case (2)* : $\tau = 0,\ \theta = \theta',\ \Gamma(0,\theta,\theta') = D(\theta)$
  This case represents the cut of ambiguity function on ($\theta = \theta'$) at zero lag where desired beamforming $D(\theta)$ will be imposed. Phase code matrix $\mathbf{P}$ controls the beampattern and frequency code $\mathbf{C}$ does not distort the pattern since each chip of $x_m(t)$ has the same frequency code during the same interval.

- *Case (3)* : $\tau = 0,\ \theta_p, \theta_q, p \neq q\ (p, q = 1 \ldots L)$ minimize $|\Gamma(0,\theta_p,\theta_q)|^2$
  This case represents the cross correlation of transmitted signals at discrete angles(targets of interest) at zero lag(same range bins). The cross correlation is only optimized for discrete angles since the power transmitted to the angles other than the targets will be low if desired beamform is implented.

3.1.1 Frequency Coding of MIMO Waveforms

For *Case (1)* we propose to use a modified Costas coding scheme which results in low autocorrelation sidelobes and thumbstack ambiguity function. Costas codes were originally developed for sonar applications by J.Costas, where the coding scheme resembles random-like frequency hopping within the pulse as opposed to LFM modulation where frequency is increasing or decreasing linearly. Figure 3.2 shows the binary matrix representation of time-frequency coding of the pulse where columns consist of K timeslices (chips) with duration t_b and rows consists of K distinct frequencies spaced by $\Delta\tilde{f}$. Each orange dot represent the occupation of a chip at corresponding delay and frequency.

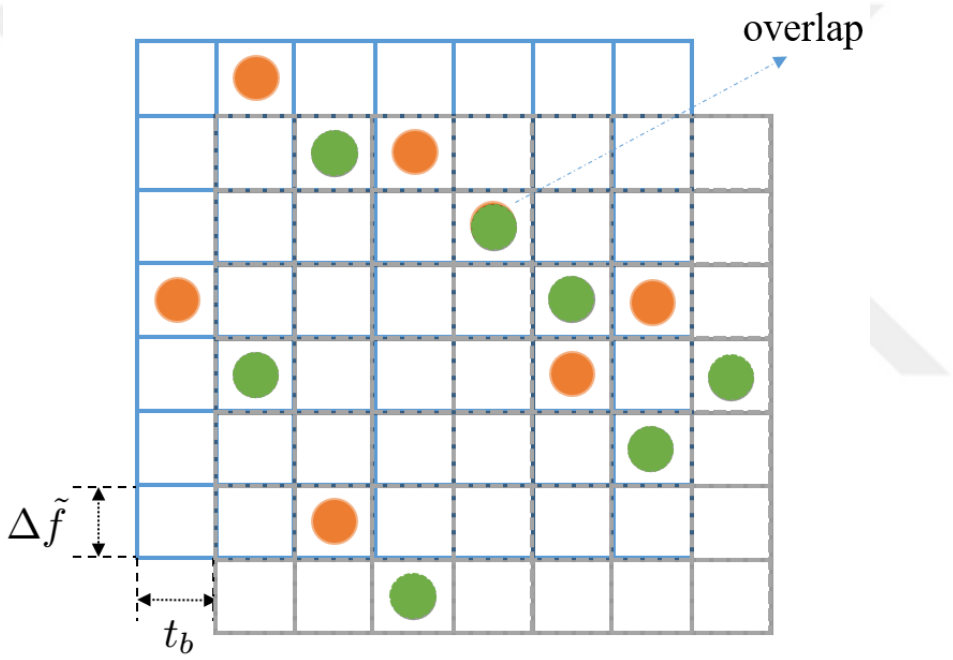

Figure 3.2: Time-Frequency Code for $K = 7$ Chips

The placement of each dot determines the hopping order and strongly affects the ambiguity function (AF) of the waveform. Since ambiguity function is the matched filter output of the range-doppler shifted version of the same signal, it can be predicted from the binary representation of the signal by overlaying a duplicate of the matrix on itself (shown by the green dots in Figure 3.2) The number of coinding dots implies ambiguity function behavior. In binary representation, first requirement is that at each chip duration only one frequency is transmitted and each frequency is used only

once. Costas set is a special subset of $K!$ possible combitations such that the number of coinciding dots can not be larger than one due to the shifting of the binary matrix in delay or doppler. This property implies a narrow peak of the ambiguity function at origin and low sidelobes elsewhere. Note that (3.6) is needed to satisfy orthonognality between the chips.

Difference matrix proposed by [2] is an effective method to create the sidelobe behavior of the Costas waveforms. Let us convert binary grid representation in Figure 3.2 to Coding matrix by placing a 1 on chips. Denoting the coding sequence as a row of frequency indexed by k ($v = k\Delta\tilde{f} \quad k = 0 \cdots K-1$), one can create a difference matrix by shifting the code sequence by different amount of delay indexed by k ($\tau = kt_b \quad k = 0 \cdots K-1$) as shown in Figure 3.3. This difference matrix means there is an overlap if a positive delay of i and doppler shift of $D_{i,j}$.

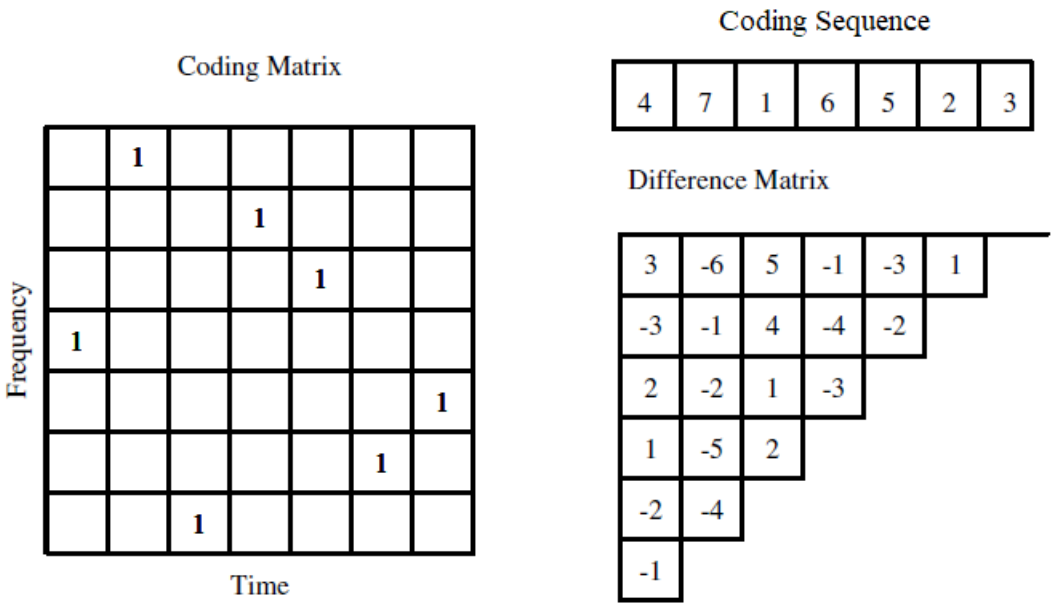

Figure 3.3: Coding and Difference Matrices for a $K = 7$ Costas Sequence

This pair $(i, D_{i,j})$ is then becomes the location of overlap at sidelobe matrix given on the right of Figure 3.4. Since the Costas sequence requires maximum number of overlapping dots as one, sidelobe matrix consists of only 1's and equivalently there must be no $D_{i,j}$ having same number in a row of difference matrix. The maximum number seen on location (0,0) is when no shifting occurs and it equals to the matrix

dimension K. Negative time delays and doppler shift can then be filled using the symmetry property of ambiguity function. Contour plot of ambiguity function on the left of Figure 3.4 is also shown to show the resemblence of sidelobe matrix.

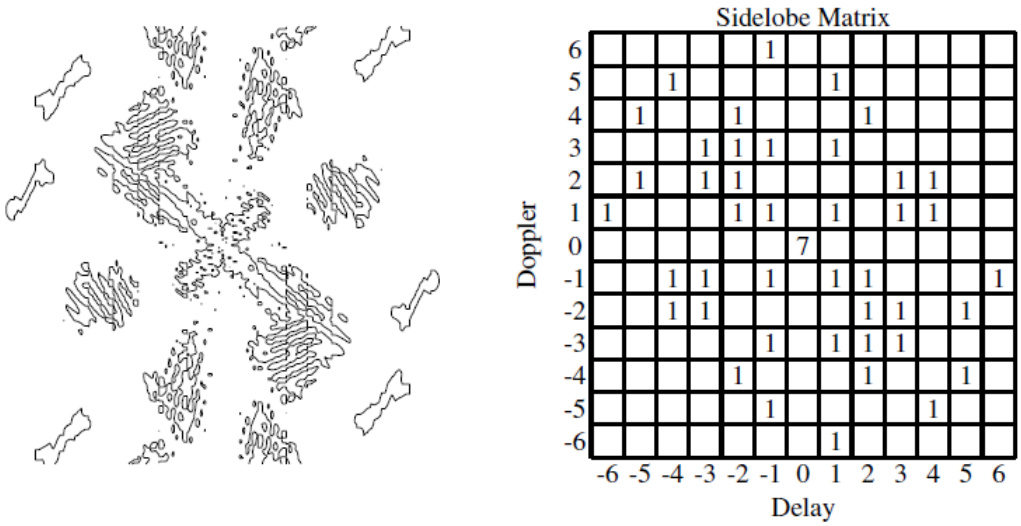

Figure 3.4: AF Contour plot and Sidelobe Matrix for a $K = 7$ Costas Sequence [2]

Exhaustive search to find Costas codes is not suitable for large codes [40]. In [41], Golomb and Taylor proposed Welch method for the construction of Costas codes for different number of chips which is adopted for this thesis. Welch 1 construction is given in [2]. It requires $p = K + 1$ order Galois field GF(p), where p is a prime number greater than 2. This restricts the coding matrix K to be a one less than a prime number. [2] provides Welch 2 and Welch 3 constructions to relax this restriction. For the purpose of Phased-Costas Coding we continue with Welch methods, further information can be found in [2]. Galois field of order p, contains a finite number of elements $\{0, 1, \cdots, p-1\}$ which obeys field properties of with respect to modulus-p. A primitive element α of a Galois field GF(p) is defined as the cyclic generator of the group where every element of the field can be expressed as primitive element raised to some integer power [2]. As an example, we demonstrate generation of Costas sequence using Welch 1 method for $K = 6$ chips. In this case, $p = K + 1 = 7$ which is prime. We write $GF(7) = 0, 1, 2, 3, 4, 5, 6$ and search for primitive element α such that for $j = 0, 1, 2 \cdots p-2$ and $i = 1, 2, \cdots p-1$ it needs to be $i = \alpha^j$.

for $\alpha = 3$

$j = 0; \quad i = 3^0 = 1$

$j = 1; \quad i = 3^1 = 3$

$j = 2; \quad i = 3^2 = 2 \text{ (mod 7)}$

$j = 3; \quad i = 3^3 = 6 \text{ (mod 7)}$

$j = 4; \quad i = 3^4 = 4 \text{ (mod 7)}$

$j = 5; \quad i = 3^5 = 5 \text{ (mod 7)}$

This sequence $\{1, 3, 2, 6, 4, 5\}$ gives Welch 1 constructed Costas sequence of $K = 6$ using primitive element $\alpha = 3$. Note that $\alpha = 2$ is not a cyclic generator of the field hence it fails to generate the sequence.

From [2], adddition of phase codes for between the chips(subpulses) will not deteriorate the resolution performance of the code. This is expected since Costas coding is already based on frequency hopping between the chips and phase change is therefore negligible and it brings us to the modified Costas coding where each phases is now optimized for the desired beampattern and its consequent constraints.

3.1.2 Phase Coding of MIMO Waveforms

We assume an optimized code for the frequency $\mathbf{C}^*$ is obtained from *Case(1)* and try to find phase codes $\mathbf{P}$ for the most general problem in (3.7). Optimization of *Case(2)* and *Case(3)* is jointly achieved by constructing a single cost function. This allows us to express the constrained minimization problem in (3.7) as a single cost function given below,

$$\begin{aligned} J\left(\mathbf{C}^*, \mathbf{P}\right) = & \frac{1}{W} \sum_{w=1}^{W} \sigma_w \left| \alpha^2 D\left(\theta_w\right) - \Gamma\left(0, \theta_w, \theta_w\right) \right|^2 \\ & + \frac{2\sigma_c}{L^2 - L} \sum_{p=1}^{L-1} \sum_{q=p+1}^{L} \left| \Gamma\left(0, \theta_p, \theta_q\right) \right|^2 \end{aligned} \tag{3.9}$$

The first part of the cost is the difference between the desired beamforming $D(\theta_w)$ (indexed by w for the interested region) and $\theta = \theta'$ cut of the ambiguity function at zero lag. The second part of the function is imposed by *Case (3)* and cross correlations of the signals transmitted to targets adds to the cost function. We need to express the above expression in terms of the Phased-Costas waveforms. To that purpose, we define $\mathbf{H}$ in terms of the samples. Let

$$\mathbf{H} = [\mathbf{h_1}, \mathbf{h_2}, \ldots, \mathbf{h_M}]_{K \times M} \tag{3.10}$$

where $\mathbf{h}_i (i = 1 \cdots M)$ is the vector form of Phased-Costas waveforms obtained from (3.1) and shown in Figure 3.1. $\mathbf{S} = \mathbf{H}^T$ is defined to obtain a suitable form for the optimization and vectorized as

$$\mathbf{S} = \mathbf{H}^T = [\mathbf{s_1}, \mathbf{s_2}, \ldots, \mathbf{s_K}]_{M \times K} \tag{3.11}$$

$$\mathbf{s} = \text{vec}(\mathbf{S}) \tag{3.12}$$

We use the matrix manipulation as in [5] to replace signal samples and steering vectors. Now the beamforming pattern $\Gamma(0, \theta_w, \theta_w) = \mathbf{a}_T^H(\theta_w)\, \mathbf{R}(0) \mathbf{a}_T(\theta_w)$ can be conveniently written as,

$$\mathbf{a}_T^H(\theta_w)\, \mathbf{R}(0) \mathbf{a}_T(\theta_w) = \mathbf{s}^H \mathbf{R}'(\theta_w)\, \mathbf{s} \tag{3.13}$$

where $\mathbf{R}'$ is defined as,

$$\mathbf{R}'(\theta) = \left(\mathbf{I_K} \otimes \mathbf{a}_T^H(\theta)\right)^H \left(\mathbf{I_K} \otimes \mathbf{a}_T^H(\theta)\right) \tag{3.14}$$

The second term in (3.9) can be similarly expressed as

$$\mathbf{a}_T^H(\theta_p)\, \mathbf{R}(0) \mathbf{a}_T(\theta_q) = \mathbf{s}^H \mathbf{R}''(\theta_p, \theta_q)\, \mathbf{s} \tag{3.15}$$

where $\mathbf{R}''$ is defined as,

$$\mathbf{R}''(\theta_p, \theta_q) = \left(\mathbf{I_K} \otimes \mathbf{a}_T^H(\theta_p)\right)^H \left(\mathbf{I_K} \otimes \mathbf{a}_T^H(\theta_q)\right) \tag{3.16}$$

Similary $\mathbf{A_1}$ and $\mathbf{A_2}$ are defined [5] to make the cost function (3.9) convert to (3.20).

$$\mathbf{A}_1(\theta_w) \triangleq \begin{pmatrix} D(\theta_w) & \mathbf{0}^T \\ \mathbf{0} & -\mathbf{R}'(\theta_w) \end{pmatrix} \tag{3.17}$$

$$\mathbf{A}_2(\theta_p, \theta_q) \triangleq \begin{pmatrix} 0 & \mathbf{0}^T \\ \mathbf{0} & \mathbf{R}''(\theta_p, \theta_q) \end{pmatrix} \tag{3.18}$$

$$\mathbf{v} \triangleq \begin{pmatrix} \alpha \\ \mathbf{s} \end{pmatrix} \tag{3.19}$$

$$\begin{aligned} J = & \frac{1}{W} \sum_{w=1}^{W} \sigma_w \left| \mathbf{v}^H \mathbf{A}_1(\theta_w) \mathbf{v} \right|^2 \\ & + \frac{2\sigma_c}{L^2 - L} \sum_{p=1}^{L-1} \sum_{q=p+1}^{L} \left| \mathbf{v}^H \mathbf{A}_2(\theta_p, \theta_q) \mathbf{v} \right|^2 \end{aligned} \tag{3.20}$$

PAR of a discrete time vector $\mathbf{h}$ of length K is defined as the ratio of peak sample power to average power.

$$PAR(\mathbf{h}) \triangleq \frac{\max_{i=1,\ldots,K} |h_i|^2}{\frac{1}{K} \sum_{i=1}^{K} |h_i|^2} = \frac{\|\mathbf{h}\|_\infty^2}{\frac{1}{K} \|\mathbf{h}\|_2^2} \tag{3.21}$$

Low PAR constraint is another feature that should be considered in the design of MIMO beamformer. Since PAR constraint is applied to the signals transmitted from the same antenna, we express it for each antenna individually. Also note that PAR is not unique as the scaling of $\mathbf{h}$ yields the same PAR. Therefore individual antenna powers are handled together with PAR constraints in order to have unique solution. We formulate the constraints to the (3.20) as (3.22)-(3.23) where $\mathbf{h}_i$ is the i-th column of (3.10).

$$\mathrm{PAR}(\mathbf{h_i}) < \delta \quad i = 1 \cdots M \tag{3.22}$$

$$\|\mathbf{h_i}\|_2^2 = c^2 \tag{3.23}$$

Since (3.20) is expressed in terms of $\mathbf{v}$, we define an operator to switch back from $\mathbf{s}$ to $\mathbf{h}_i$ for expressing the constraints easily. Let $\mathbf{E} = [\mathbf{0},\ \mathbf{I}_{MK}]$ is the matrix to select $\mathbf{s}$ from $\mathbf{v}$. Operator L_i maps vectorized signal $\mathbf{s}$ back to $\mathbf{h}_i$ as defined in (3.25) where $\mathbf{T}_i$ size $K \times M$ zero matrix except at $T_{ii} = 1$.

$$\mathbf{E}\mathbf{v} = \mathbf{s} \tag{3.24}$$

$$L_i : \mathbb{C}^{MK\times 1} \rightarrow \mathbb{C}^{K\times 1}, i = 1 \cdots M$$

$$L_i(\mathbf{s}) = (\mathrm{vec}^{-1}(\mathbf{s}))^T \mathbf{T}_i = \mathbf{h}_i \tag{3.25}$$

Summarizing the phase code optimization problem with PAR constraints,

$$\min_{\mathbf{v}} \frac{1}{W} \sum_{w=1}^{W} \sigma_w \left|\mathbf{v}^H \mathbf{A}\left(\theta_w\right)\mathbf{v}\right|^2 \tag{3.26}$$

$$+ \frac{2\sigma_c}{L^2 - L} \sum_{p=1}^{L-1} \sum_{q=p+1}^{L} \left|\mathbf{v}^H \mathbf{A}\left(\theta_p, \theta_q\right)\mathbf{v}\right|^2 \tag{3.27}$$

$$\textit{s.t}\ \ \mathrm{PAR}(\mathbf{h}_i) \leq \delta \quad i = 1 \cdots M \tag{3.28}$$

$$\|\mathbf{h}_i\|^2 = c^2 \tag{3.29}$$

where $L_i(\mathbf{E}\mathbf{v}) = \mathbf{h}_i$. Notice that objective function (3.26) is fourth order nonconvex polynomial function and PAR constraint (3.28) and (3.29) specifies nonconvex set making the complexity of the problem NP-hard [31], [42].

3.2 MIMO Waveform Design

3.2.1 A brief overview of ADMM Method

The ADMM blends the decomposability of dual ascent and superior convergence properties of the method of multipliers [43], [44]. The basic form that it is applied

$$\begin{aligned} \text{minimize} \quad & f(x) + g(z) \\ \text{subject to} \quad & Ax + Bz = c \end{aligned} \tag{3.30}$$

where $x \in \mathbf{R}^n$, $z \in \mathbf{R}^m$ and $A \in \mathbf{R}^{p\times n}$, $B \in \mathbf{R}^{p\times m}$ and $c \in \mathbf{R}^p$. Notice that objective function is split into two parts and f and g are assumed convex. The optimal value

$$p^\star = \inf\{f(x) + g(z) \mid Ax + Bz = c\} \tag{3.31}$$

can be found by ADMM iterations

$$x^{k+1} := \underset{x}{\operatorname{argmin}}\, L_\rho\left(x, z^k, y^k\right) \tag{3.32a}$$

$$z^{k+1} := \underset{z}{\operatorname{argmin}}\, L_\rho\left(x^{k+1}, z, y^k\right) \tag{3.32b}$$

$$y^{k+1} := y^k + \rho\left(Ax^{k+1} + Bz^{k+1} - c\right) \tag{3.32c}$$

where $\rho > 0$ and augmented Lagrangian is defined as

$$L_\rho(x, z, y) = f(x) + g(z) + y^T(Ax + Bz - c) + (\rho/2)\|Ax + Bz - c\|_2^2 \tag{3.33}$$

The algorithm consists of an x-minimization (3.32a), a z-minimization (3.32b), and a dual variable update (3.32c) with step size equal to the augmented Lagrangian parameter ρ.

Combining the linear and quadratic terms in the augmented Lagrangian and scaling the dual variable $u = (1/\rho)y$, ADMM updates can be written in *scaled* form. Let the residual be defined as $r = Ax + Bz - c$, the last two term in (3.33) can be written as [43] :

$$y^T r + (\rho/2)\|r\|_2^2 = (\rho/2)\|r + (1/\rho)y\|_2^2 - (1/2\rho)\|y\|_2^2 \tag{3.34}$$

$$= (\rho/2)\|r + u\|_2^2 - (\rho/2)\|u\|_2^2 \tag{3.35}$$

and updates become

$$x^{k+1} := \underset{x}{\operatorname{argmin}} \left(f(x) + (\rho/2) \left\| Ax + Bz^k - c + u^k \right\|_2^2 \right) \tag{3.36}$$

$$z^{k+1} := \underset{z}{\operatorname{argmin}} \left(g(z) + (\rho/2) \left\| Ax^{k+1} + Bz - c + u^k \right\|_2^2 \right) \tag{3.37}$$

$$u^{k+1} := u^k + Ax^{k+1} + Bz^{k+1} - c. \tag{3.38}$$

Under assumptions that f and g are *closed*, *proper* and *convex* and the unaugmented Lagrangian has a saddle point, ADMM iterations satisfy the following [43]:

- Residual convergence. $r^k \to 0$ as $k \to \infty$.
- Objective convergence. $f\left(x^k\right) + g\left(z^k\right) \to p^\star$ as $k \to \infty$
- Dual variable convergence. $y^k \to y^\star$ as $k \to \infty$, where $y^\star$ is dual optimal point.

Stopping thresholds for $\|x^k\| \leq \epsilon^{\text{pri}}$ and $\|y^k\| \leq \epsilon^{\text{dual}}$ for primal and dual variables are given as [43]:

$$\epsilon^{\text{pri}} = \sqrt{p}\epsilon^{\text{abs}} + \epsilon^{\text{rel}} \max\left\{ \left\| Ax^k \right\|_2, \left\| Bz^k \right\|_2, \|c\|_2 \right\} \tag{3.39}$$

$$\epsilon^{\text{dual}} = \sqrt{n}\epsilon^{\text{abs}} + \epsilon^{\text{rel}} \left\| A^T y^k \right\|_2 \tag{3.40}$$

where $\epsilon^{\text{abs}} > 0$ is an absolute tolerance and $\epsilon^{\text{rel}} > 0$ is a relative.

Biconvex objective functions can also be solved with ADMM

$$\begin{array}{ll} \text{minimize} & F(x, z) \\ \text{subject to} & G(x, z) = 0 \end{array} \tag{3.41}$$

where $F : \mathbf{R}^n \times \mathbf{R}^m \to \mathbf{R}$ is bi-convex, i.e., convex in x for each z and convex in z for each x, and $G : \mathbf{R}^n \times \mathbf{R}^m \to \mathbf{R}^p$ is bi-affine, i.e., affine in x for each fixed z, and affine in z for each fixed x and updates become [43]:

$$x^{k+1} := \underset{x}{\operatorname{argmin}} \left(F\left(x, z^k\right) + (\rho/2) \left\| G\left(x, z^k\right) + u^k \right\|_2^2 \right) \tag{3.42}$$

$$z^{k+1} := \underset{z}{\operatorname{argmin}} \left(F\left(x^{k+1}, z\right) + (\rho/2) \left\| G\left(x^{k+1}, z\right) + u^k \right\|_2^2 \right) \tag{3.43}$$

$$u^{k+1} := u^k + G\left(x^{k+1}, z^{k+1}\right) \tag{3.44}$$

3.2.2 Application of ADMM to MIMO Waveforms

For ADMM formulation, we construct two primal variables as $\mathbf{v}_1$, $\mathbf{v}_2$ for the decoupling of (3.26). Writing the objective function (3.26) in two primal variables $\mathbf{v_1}, \mathbf{v_2}$, (3.26) is turned to a bi-convex function of $\mathbf{v}_1$ and $\mathbf{v}_2$ as (3.45a). In addition, two primal variables $\mathbf{q}_1$ and $\mathbf{q}_2$ are defined for PAR and energy constraints in (3.28) and (3.29). The resulting optimization problem in four primal variables becomes

$$\min_{\mathbf{v_1},\mathbf{v_2}} \frac{1}{W}\sum_{w=1}^{W}\sigma_w \left|\mathbf{v_1}^H\mathbf{A}\left(\theta_w\right)\mathbf{v_2}\right|^2 \tag{3.45a}$$

$$+\frac{2\sigma_c}{L^2-L}\sum_{p=1}^{L-1}\sum_{q=p+1}^{L}\left|\mathbf{v_1}^H\mathbf{A}\left(\theta_p,\theta_q\right)\mathbf{v_2}\right|^2$$

$$s.t\ \ \mathbf{v_1}-\mathbf{v_2}=\mathbf{0} \tag{3.45b}$$

$$\mathbf{E}\mathbf{v_1}=\mathbf{q}_1 \tag{3.45c}$$

$$\mathbf{E}\mathbf{v_2}=\mathbf{q}_2 \tag{3.45d}$$

$$\text{PAR}(\mathbf{q}_{1i})\le\delta\,,\quad i=1\cdots M \tag{3.45e}$$

$$\|\mathbf{q}_{1i}\|_2^2=c^2 \tag{3.45f}$$

$$\text{PAR}(\mathbf{q}_{2i})\le\delta\,,\quad i=1\cdots M \tag{3.45g}$$

$$\|\mathbf{q}_{2i}\|_2^2=c^2 \tag{3.45h}$$

where $\mathbf{q}_{1i}=L_i(\mathbf{q}_1)$ and $\mathbf{q}_{2i}=L_i(\mathbf{q}_2)$ for $i=1\cdots M$. Denoting the objective function in (3.45) as

$$F(\mathbf{v_1},\mathbf{v_2})=\frac{1}{W}\sum_{w=1}^{W}\sigma_w\left|\mathbf{v_1}^H\mathbf{A}\left(\theta_w\right)\mathbf{v_2}\right|^2+\frac{2\sigma_c}{L^2-L}\sum_{p=1}^{L-1}\sum_{q=p+1}^{L}\left|\mathbf{v_1}^H\mathbf{A}\left(\theta_p,\theta_q\right)\mathbf{v_2}\right|^2 \tag{3.46}$$

The augmented Lagrangian is defined as

$$\begin{aligned}\mathcal{L}(\mathbf{v_1},\mathbf{v_2},\mathbf{q_1},\mathbf{q_2},\mathbf{y_1},\mathbf{y_2},\mathbf{y_3}) &= F(\mathbf{v_1},\mathbf{v_2})\\ &+\text{Re}\{\mathbf{y}_1^H(\mathbf{v_1}-\mathbf{v_2})\}+\frac{\rho_1}{2}\|\mathbf{v_1}-\mathbf{v_2}\|_2^2\\ &+\text{Re}\{\mathbf{y}_2^H(\mathbf{E}\mathbf{v_1}-\mathbf{q_1})\}+\frac{\rho_2}{2}\|\mathbf{E}\mathbf{v_1}-\mathbf{q_1}\|_2^2\\ &+\text{Re}\{\mathbf{y}_3^H(\mathbf{E}\mathbf{v_2}-\mathbf{q_2})\}+\frac{\rho_3}{2}\|\mathbf{E}\mathbf{v_2}-\mathbf{q_2}\|_2^2\end{aligned} \tag{3.47}$$

where ρ_1, ρ_2, ρ_3 are scalars for the penalty terms. By completing the squares, auxillary variables $\mathbf{y}_1, \mathbf{y}_2, \mathbf{y}_3$ can be taken into norm squared terms and written in *scaled form*

$$\begin{aligned}\mathcal{L}(\mathbf{v_1}, \mathbf{v_2}, \mathbf{q_1}, \mathbf{q_2}, \mathbf{y_1}, \mathbf{y_2}, \mathbf{y_3}) &= F(\mathbf{v_1}, \mathbf{v_2}) \\ &+ \frac{\rho_1}{2}\|\mathbf{v_1} - \mathbf{v_2} + \frac{1}{\rho_1}\mathbf{y_1}\|_2^2 + \frac{\rho_2}{2}\|\mathbf{E}\mathbf{v_1} - \mathbf{q_1} + \frac{1}{\rho_2}\mathbf{y_2}\|_2^2 \\ &+ \frac{\rho_3}{2}\|\mathbf{E}\mathbf{v_2} - \mathbf{q_2} + \frac{1}{\rho_3}\mathbf{y_3}\|_2^2 + C\end{aligned} \tag{3.48}$$

where C is a constant, independent of primal variables. Further simplification is achieved by defining the following terms, i.e.,

$$\mathbf{u} = \frac{1}{\rho_1}\mathbf{y_1} \qquad \mathbf{w} = \frac{1}{\rho_2}\mathbf{y_2} \qquad \mathbf{z} = \frac{1}{\rho_3}\mathbf{y_3} \tag{3.49}$$

Using scaled variables (3.49) in (3.48), the most compact form of the augmented Lagrangian in (3.50) can be written as,

$$\begin{aligned}\mathcal{L}(\mathbf{v_1}, \mathbf{v_2}, \mathbf{q_1}, \mathbf{q_2}, \mathbf{u}, \mathbf{w}, \mathbf{z}) = F(\mathbf{v_1}, \mathbf{v_2}) + \frac{\rho_1}{2}\|\mathbf{v_1} - \mathbf{v_2} + \mathbf{u}\|_2^2 \\ + \frac{\rho_2}{2}\|\mathbf{E}\mathbf{v_1} - \mathbf{q_1} + \mathbf{w}\|_2^2 + \frac{\rho_3}{2}\|\mathbf{E}\mathbf{v_2} - \mathbf{q_2} + \mathbf{z}\|_2^2\end{aligned} \tag{3.50}$$

Notice that update of $\mathbf{q}_1$ (3.51a) and $\mathbf{q}_2$ (3.51b) only depends on the third and fourth term in total augmented Lagrangian given in (3.50). All primal and dual updates are expressed from (3.51a) to (3.51g).

$$\mathbf{q}_1^{m+1} := \arg\min_{\mathbf{q}_1} \|\mathbf{q}_1 - (\mathbf{E}\mathbf{v_1}^m + \mathbf{w}^m)\|_2^2 \tag{3.51a}$$

$$\mathbf{q}_2^{m+1} := \arg\min_{\mathbf{q}_2} \|\mathbf{q}_2 - (\mathbf{E}\mathbf{v_2}^m + \mathbf{z}^m)\|_2^2 \tag{3.51b}$$

$$\mathbf{v}_1^{m+1} := \arg\min_{\mathbf{v}_1} \mathcal{L}\left(\mathbf{v_1}, \mathbf{v_2}^m, \mathbf{q_1}^{m+1}, \mathbf{q_2}^{m+1}, \mathbf{u}^m, \mathbf{w}^m, \mathbf{z}^m\right) \tag{3.51c}$$

$$\mathbf{v}_2^{m+1} := \arg\min_{\mathbf{v}_2} \mathcal{L}\left(\mathbf{v_1}^{m+1}, \mathbf{v_2}, \mathbf{q_1}^{m+1}, \mathbf{q_2}^{m+1}, \mathbf{u}^m, \mathbf{w}^m, \mathbf{z}^m\right) \tag{3.51d}$$

$$\mathbf{u}^{m+1} := \mathbf{u}^m + \mathbf{v_1}^{m+1} - \mathbf{v_2}^{m+1} \tag{3.51e}$$

$$\mathbf{w}^{m+1} := \mathbf{w}^m + \mathbf{E}\mathbf{v_1}^{m+1} - \mathbf{q_1}^{m+1} \tag{3.51f}$$

$$\mathbf{z}^{m+1} := \mathbf{z}^m + \mathbf{E}\mathbf{v_2}^{m+1} - \mathbf{q_2}^{m+1} \tag{3.51g}$$

The updates of $\mathbf{q_1}$ and $\mathbf{q_2}$ with the PAR constraints (3.45e)-(3.45h) are separately considered. Since the PAR constraint is applied to the samples of the signal from the same antenna, (3.51a) can be rearranged as

$$\begin{aligned}
&\arg\min_{\mathbf{q}_1} \|\mathbf{q}_1 - (\mathbf{E}{\mathbf{v_1}}^m + \mathbf{w}^m)\|_2^2 \\
&= \sum_{i=1}^{M} \arg\min_{\mathbf{q}_1} \|L_i(\mathbf{q}_1 - (\mathbf{E}{\mathbf{v_1}}^m + \mathbf{w}^m))\|_2^2 \\
&= \sum_{i=1}^{M} \arg\min_{\mathbf{q}_{1i}} \|\mathbf{q}_{1i} - L_i(\mathbf{E}{\mathbf{v_1}}^m + \mathbf{w}^m))\|_2^2
\end{aligned} \tag{3.52}$$

where $\mathbf{q}_{1i} = L_i(\mathbf{q}_1)$. Here we continue to the update of (3.51a), but the updates of (3.51b) can be written similary. Let $\mathbf{q}$ be the nearest vector with desired PAR value δ and energy c^2. We formulate the optimization problem as

$$\min_{\mathbf{q}} \|\mathbf{q} - \mathbf{r}\|_2^2 \tag{3.53a}$$

$$\text{s.t.} \quad \mathrm{PAR}(\mathbf{q}) \leq \delta \tag{3.53b}$$

$$\|\mathbf{q}\|_2^2 = c^2 \tag{3.53c}$$

Notice that objective function in (3.53a) is same as the inner terms of (3.52) with $\mathbf{q} = \mathbf{q}_{1i}$, $\mathbf{r} = L_i(\mathbf{E}{\mathbf{v_1}}^m + \mathbf{w}^m)$ $i = 1 \cdots M$. (3.53b) and (3.53c) ensure the constraints defined in (3.45e) and (3.45f). This problem is still nonconvex and needs to be solved. Expanding (3.53a) and defining unit norm vector $\tilde{\mathbf{s}}$, let $\mathbf{q} = c\,\tilde{\mathbf{s}}$ where $c > 0$, we reformulate the problem as

$$\min_{\tilde{\mathbf{s}}} \quad c^2 - 2c\,\mathrm{Re}(\tilde{\mathbf{s}}^H\mathbf{r}) + \|\mathbf{r}\|_2^2 \tag{3.54a}$$

$$\text{s.t.} \quad |\tilde{s_k}|^2 \leq \frac{\delta}{K}, \quad k = 1 \ldots K \tag{3.54b}$$

$$\|\tilde{\mathbf{s}}\|_2^2 = 1 \tag{3.54c}$$

where PAR constraint in (3.53b) turns to (3.54b) in terms of the elements of unit norm vector $\tilde{\mathbf{s}}$. Since for any $\mathbf{q}$ with fixed c, (3.53a) can only be minimized when $\mathrm{Re}(\tilde{\mathbf{s}}^H\mathbf{r})$

is maximized, (3.54) can be rewritten as

$$\max_{\tilde{\mathbf{s}}} \mathrm{Re}(\tilde{\mathbf{s}}^H \mathbf{r}) \tag{3.55a}$$

$$\text{s.t.} \quad |\tilde{s_k}|^2 \leq \frac{\delta}{K}, \quad k = 1 \dots K \tag{3.55b}$$

$$\|\tilde{\mathbf{s}}\|_2^2 = 1 \tag{3.55c}$$

In [8], it is proven that nonconvex constraint (3.55c) can be written as (3.56c) and have the same optimal solution. This is expected since the objective function (3.56a) pulls the solution to the upper bound by adding an increment $\Delta\mathbf{r}$ even if it is defined with less than or equal to constraint as in (3.56c). Therefore equation set (3.56a)-(3.56c) is now second order cone problem (SOCP) and convex.

$$\max_{\tilde{\mathbf{s}}} \mathrm{Re}(\tilde{\mathbf{s}}^H \mathbf{r}) \tag{3.56a}$$

$$\text{s.t.} \quad |\tilde{s_k}|^2 \leq \frac{\delta}{K}, \quad k = 1 \dots K \tag{3.56b}$$

$$\|\tilde{\mathbf{s}}\|_2^2 \leq 1 \tag{3.56c}$$

The problem in (3.56) can be solved with any public convex solver but in [8], more efficient solution is proposed which is adopted in this paper. In (3.57) the solution to update equation (3.51a) is given for all $\mathbf{r} = L_i(\mathbf{E}{\mathbf{v_1}}^m + \mathbf{w}^m)$, $i = 1 \cdots M$ as $\mathbf{q}_{1i}^{m+1} = c\,\tilde{\mathbf{s}}$ and primal variable is updated as $\mathbf{q}_1^{m+1} = \mathrm{vec}([\mathbf{q}_{11}^{m+1} \dots \mathbf{q}_{1M}^{m+1}]^T)$. Same steps are applied for (3.51b) with the only difference being $\mathbf{r} = L_i(\mathbf{E}{\mathbf{v_2}}^m + \mathbf{z}^m)$, $i = 1 \cdots M$ and $\mathbf{q}_2^{m+1} = \mathrm{vec}([\mathbf{q}_{21}^{m+1} \dots \mathbf{q}_{2M}^{m+1}]^T)$. The Lagrangian multiplier γ is found using simple binary search as proposed in [8] and given in Appendix A.

$$\tilde{s_k} = \begin{cases} \frac{r_k}{2\gamma}, & \frac{|r_k|}{2\gamma} < \sqrt{\frac{\delta}{K}} \\ \sqrt{\frac{\delta}{K}} e^{j\phi(r_k)}, & \text{otherwise} \end{cases} \tag{3.57}$$

For the updates of (3.51c) and (3.51d) closed form solutions (3.58a) and (3.59a) exist and derivations are given in Appendix B.

$$\mathbf{v_1^{m+1}} = \left(\mathbf{C_1} + \frac{\rho_1}{2}\mathbf{I} + \frac{\rho_2}{2} \begin{bmatrix} 0 \\ \mathbf{E} \end{bmatrix} \right)^{-1} \left(\frac{\rho_1}{2}(\mathbf{v_2}^m - \mathbf{u}^m) + \begin{bmatrix} 0 \\ \frac{\rho_2}{2}(\mathbf{q_1}^{m+1} - \mathbf{w}^m) \end{bmatrix} \right) \tag{3.58a}$$

$$\mathbf{C_1} \triangleq \frac{1}{W}\sum_{w=1}^{W} \sigma_w \mathbf{A}_1(\theta_w)\, \mathbf{v_2}^m \mathbf{v_2}^{mH} \mathbf{A}_1^H(\theta_w) + \frac{2\sigma_c}{L^2 - L}\sum_{p=1}^{L-1}\sum_{q=p+1}^{L} \mathbf{A}_2(\theta_p, \theta_q)\, \mathbf{v_2}^m \mathbf{v_2}^{mH} \mathbf{A}_2^H(\theta_p, \theta_q) \tag{3.58b}$$

$$\mathbf{v_2^{m+1}} = \left(\mathbf{C_2} + \frac{\rho_1}{2}\mathbf{I} + \frac{\rho_3}{2} \begin{bmatrix} 0 \\ \mathbf{E} \end{bmatrix} \right)^{-1} \left(\frac{\rho_1}{2}(\mathbf{v_1}^{m+1} + \mathbf{u}^m) + \begin{bmatrix} 0 \\ \frac{\rho_3}{2}(\mathbf{q_2}^{m+1} - \mathbf{z}^m) \end{bmatrix} \right) \tag{3.59a}$$

$$\mathbf{C_2} \triangleq \frac{1}{W}\sum_{w=1}^{W} \sigma_w \mathbf{A}_1^H(\theta_w)\, \mathbf{v_1}^{m+1} \mathbf{v_1}^{m+1H} \mathbf{A}_1(\theta_w) + \frac{2\sigma_c}{L^2 - L}\sum_{p=1}^{L-1}\sum_{q=p+1}^{L} \mathbf{A}_2^H(\theta_p, \theta_q)\, \mathbf{v_1}^{m+1} \mathbf{v_1}^{m+1H} \mathbf{A}_2(\theta_p, \theta_q) \tag{3.59b}$$

The dual updates are as follows:

$$\mathbf{u}^{m+1} = \mathbf{u}^m + (\mathbf{v_1}^{m+1} - \mathbf{v_2}^{m+1}) \tag{3.60}$$

$$\mathbf{w}^{m+1} = \mathbf{w}^m + (\mathbf{E}\mathbf{v_1}^{m+1} - \mathbf{q_1}^{m+1}) \tag{3.61}$$

$$\mathbf{z}^{m+1} = \mathbf{z}^m + (\mathbf{E}\mathbf{v_2}^{m+1} - \mathbf{q_2}^{m+1}) \tag{3.62}$$

At iteration step $m+1$ primal and dual residuals are as follows:

$$\mathbf{p}_{r1}^{m+1} = \mathbf{v}_1^{m+1} - \mathbf{v}_2^{m+1} \tag{3.63a}$$

$$\mathbf{p}_{r2}^{m+1} = \mathbf{E}\mathbf{v}_1^{m+1} - \mathbf{q}_1^{m+1} \tag{3.63b}$$

$$\mathbf{p}_{r3}^{m+1} = \mathbf{E}\mathbf{v}_2^{m+1} - \mathbf{q}_2^{m+1} \tag{3.63c}$$

$$\mathbf{d}_{r1}^{m+1} = \rho_1(\mathbf{v}_1^{m+1} - \mathbf{v}_1^{m}) \tag{3.63d}$$

$$\mathbf{d}_{r2}^{m+1} = \rho_2(\mathbf{E}\mathbf{v}_1^{m+1} - \mathbf{E}\mathbf{v}_1^{m}) \tag{3.63e}$$

$$\mathbf{d}_{r3}^{m+1} = \rho_3(\mathbf{E}\mathbf{v}_2^{m+1} - \mathbf{E}\mathbf{v}_2^{m}) \tag{3.63f}$$

Using [43], termination criterions for the optimization of (3.45) can be given where $\epsilon_{abs} > 0$ and $\epsilon_{rel} > 0$ denotes absolute and relative tolerance levels. In (3.64) we consider the convergence of $\mathbf{v}_1$ to $\mathbf{v}_2$ and $\mathbf{E}\mathbf{v}_1$ to $\mathbf{q}_1$ for brevity.

$$\|\mathbf{p}_{r1}^{m+1}\|_2^2 \leq \epsilon_1 \, , \|\mathbf{p}_{r2}^{m}\|_2^2 \leq \epsilon_2 \, , \|\mathbf{d}_{r1}^{m}\|_2^2 \leq \epsilon_3 \, , \|\mathbf{d}_{r2}^{m}\|_2^2 \leq \epsilon_4 \tag{3.64}$$

where

$$\epsilon_1 = \sqrt{MK+1}\ \epsilon_{abs} + \epsilon_{rel} \max(\|\mathbf{v}_1\|_2, \|\mathbf{v}_2\|_2) \tag{3.65a}$$

$$\epsilon_2 = \sqrt{MK}\ \epsilon_{abs} + \epsilon_{rel} \max(\|\mathbf{E}\mathbf{v}_1\|_2, \|\mathbf{q}_1\|_2) \tag{3.65b}$$

$$\epsilon_3 = \sqrt{MK+1}\ \epsilon_{abs} + \epsilon_{rel}\|\rho_1\mathbf{u}\|_2) \tag{3.65c}$$

$$\epsilon_4 = \sqrt{MK}\ \epsilon_{abs} + \epsilon_{rel}\|\rho_2\mathbf{w}\|_2) \tag{3.65d}$$

3.2.3 PCC-PAR Algorithm

The algorithm for solving problem (3.45) is given. It is reasonble to choose penalty terms ρ_2 and ρ_3 as equal since $\mathbf{q}_1$ and $\mathbf{q}_2$ are meant to converge to same point with equal priority.

Algorithm 1: PCC-PAR

Initialize $\mathbf{v}_1^0, \mathbf{v}_2^0, \mathbf{q}_1^0, \mathbf{q}_2^0, \mathbf{u}^0, \mathbf{w}^0, \mathbf{z}^0, \rho_1, \rho_2 = \rho_3, \delta, c$, and the tolerances ϵ_{abs} and ϵ_{rel} ;

while $\|\mathbf{p}_{r1}^m\|_2^2 \leq \epsilon_1$ *not satisfied* **do**

- Update $\mathbf{q}_{1i}^{m+1}$ using (3.57) for all $\mathbf{r} = L_i(\mathbf{E}{\mathbf{v_1}}^m + \mathbf{w}^m)$, $i = 1 \cdots M$;
- Find $\mathbf{q}_1^{m+1} = \mathrm{vec}([\mathbf{q}_{11}^{m+1} \ldots \mathbf{q}_{1M}^{m+1}]^T)$;
- Update $\mathbf{q}_{2i}^{m+1}$ using (3.57) for all $\mathbf{r} = L_i(\mathbf{E}{\mathbf{v_2}}^m + \mathbf{z}^m)$, $i = 1 \cdots M$;
- Find $\mathbf{q}_2^{m+1} = \mathrm{vec}([\mathbf{q}_{21}^{m+1} \ldots \mathbf{q}_{2M}^{m+1}]^T)$;
- Update $\mathbf{v}_1^{m+1}$ using (3.58a) ;
- Update $\mathbf{v}_2^{m+1}$ using (3.59a) ;
- Update $\mathbf{u}^{m+1}$ using (3.60) ;
- Update $\mathbf{w}^{m+1}$ using (3.61) ;
- Update $\mathbf{z}^{m+1}$ using (3.62) ;
- $\mathrm{m} = \mathrm{m} + 1$;

end

CHAPTER 4

NUMERICAL EXAMPLES

We demonsrate the performance of the codes with a collocated MIMO radar involving $M = 11$ ULA elements with half-wavelength spacing. The array is used for both transmit and receive. Consider the case with $L = 3$ targets located at $\theta_1 = -40$, $\theta_2 = 0$, $\theta_3 = 40$. Using $\{\theta_l\}_{l=1}^{L}$ for desired beampattern with $\Delta\theta = 12^\circ$, $D(\theta_w)$ is constructed for the range $[-80, 80]$ with 1° spacing indexed by w. We use the same energy level to all antennas (i.e $c^2 = 1$ for $m = 1 \cdots M$). The weights in (3.45) is chosen as $\sigma_w = 1$ for all $w \in W$. $\sigma_c = 1$ is chosen for the minimization of spatial cross correlation. ADMM is applied for $K = 12$ chips initially with $\rho_1 = \rho_2 = \rho_3 = 20$ as the penalty parameters and tolerance levels of $\epsilon_{abs} = 10^{-3}$ and $\epsilon_{rel} = 10^{-2}$. Primal variables $\mathbf{v}_1^0$, $\mathbf{v}_2^0$, $\mathbf{q}_1^0$, $\mathbf{q}_2^0$ are initialized to be unit norm random vector and dual variables $\mathbf{u}^0$, $\mathbf{w}^0$, $\mathbf{z}^0$ are initialized to be zero vector. In addition to the optimum solutions in the following simulations, we include in Appendix D the inferior/suboptimum approaches found in literature where ADMM is applied without PAR constraint and closest point satisfying PAR is then chosen.

4.1 Convergence

The optimization was run up to 150 iterations to show the progress of the convergence. Figure 4.1(a) shows the cost function with respect to relative weights of penalty parameters. Notice that when priority of PAR constraint is greater (i.e $\rho_2 = \rho_3 > \rho_1$) the damping behavior of is more clearer. In all cases, cost function becomes steady after 100 iterations. Figure 4.1(b) shows residues in semilog scale. All residues become less than 10^{-2} after 100 iterations.

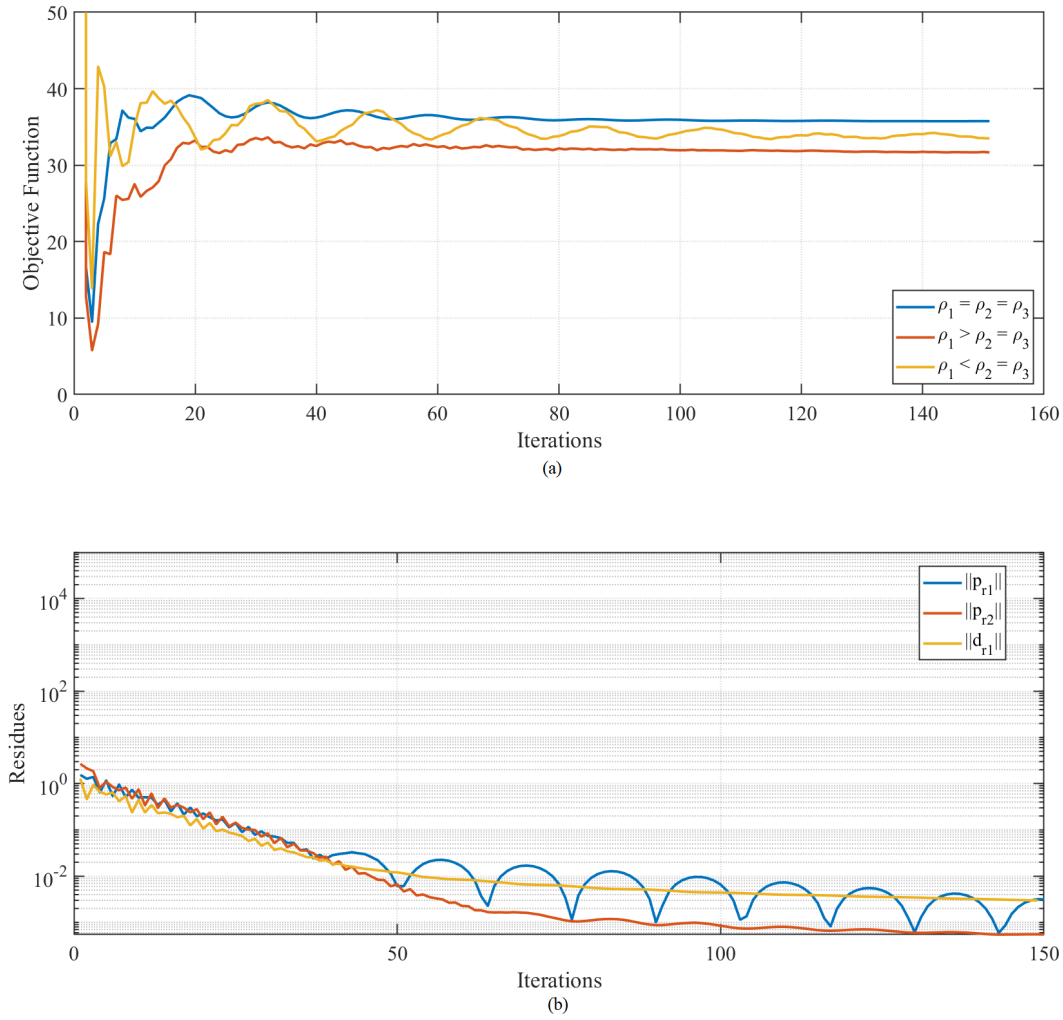

Figure 4.1: (a) Convergence with respect to penalty parameters and (b) Residues for the $\rho_1 = \rho_2 = \rho_3$ case

4.2 Time-Frequency Codes

After the convergence, signal parameters (amplitude and phase) are extracted from PCC-PAR solutions. For frequency codes, 12 chip Costas code $\mathbf{C} = \{1, 2, 4, 8, 3, 6, 12, 11, 9, 5, 10, 7\}$ with duration $t_b = 2.56\,\mu s$ and frequency hop size $\Delta\tilde{f} = 1$ MHz is implemented. Figure 4.2 shows the STFT for the time-frequency distribution of the codes with sampling frequency $f_s = 100$ MHz and total pulse width as $T_x = 30.72\mu s$. Note that orthogonality condition (3.6) between the chips is satified with a margin. The total bandwidth for PCC set is therefore 12 MHz satisfying temporal properties of Costas codes.

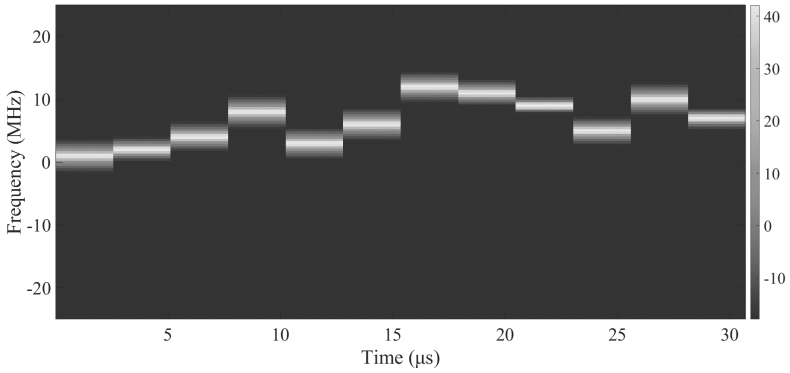

Figure 4.2: Time-frequency distribution of $K = 12$ Chip Phased-Costas Coded Waveform with total pulse width as $T_x = 30.72\mu s$ and chip size $2.56\mu s$ with total bandwith of 12MHz

4.3 Multibeam Solutions

Figure 4.3 shows the resulting optimum beampattern solutions with respect to different PAR values. Note that PAR value $\delta = 1$ corresponds to phase-only solution. This property is very desirable to make the PCC set constant envelope signal, therefore β_{m_k} can be fixed in (3.1). Mean square error between normalized desired pattern and solution is given in Table I in addition to normalized cross correlation costs which is also minimized in (3.45). Notice that as PAR values are relaxed(increased) costs might be reduced further.

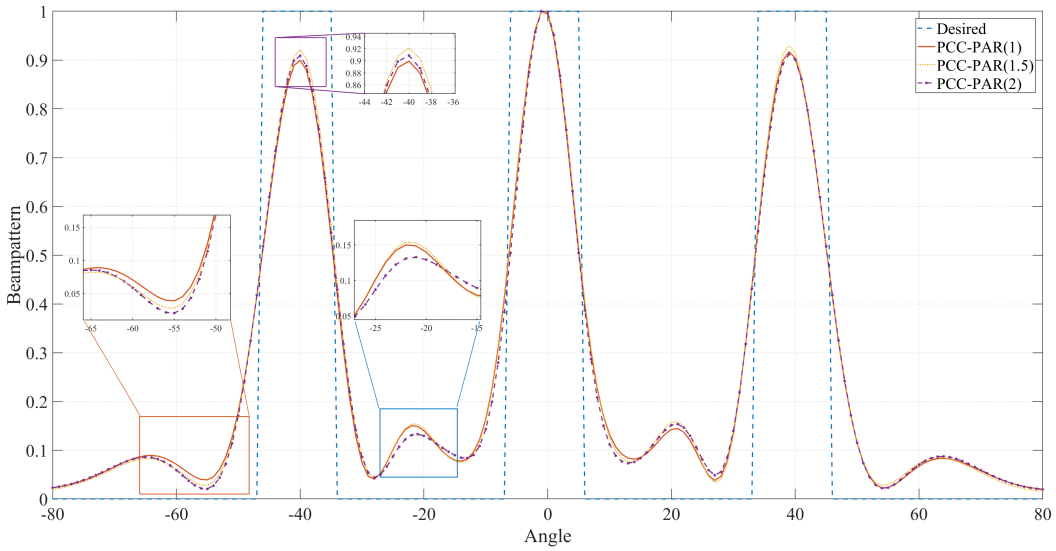

Figure 4.3: Multibeam PCC-PAR Solutions for $\delta = 1, 1.5, 2$

Table 4.1: MSE and Cross Correlation Costs of PCC-PAR

	δ	MSE	Σ XCorr
PCC-PAR	1	0.0346	0.0424
PCC-PAR	1.2	0.0342	0.0252
PCC-PAR	1.5	0.0337	0.0249
PCC-PAR	2	0.0329	0.0246

Figure 4.4 shows the PCC-PAR beampattern with other studies. The method reaches the same optimum solution with that of covariance matrix $\mathbf{R}$ method [3] and constant modulus implementation of [5]. All solutions converge to the same optimum points under same conditions. The advantage of the proposed method compared to the covariance matrix optimization is that PCC-PAR directly produces signal samples however covariance matrix approach requires additional optimization to produce signal samples. Suboptimum beampattern based on the covariance matrix using Cylic Adaptive(CA) method [4] is also plotted. PCC-PAR is also compared to DFT based method [6] which results slightly poorer when antenna number is limited.

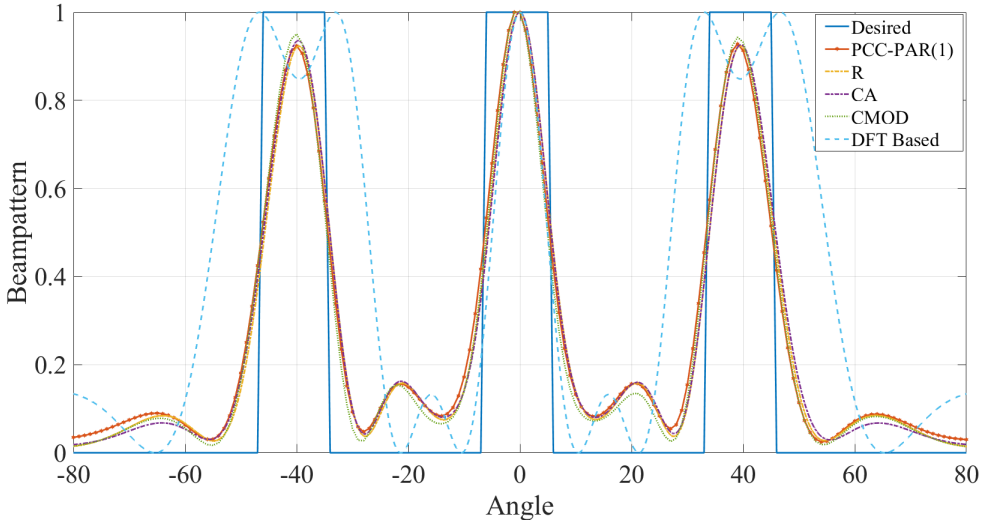

Figure 4.4: PCC-PAR(1) beampattern vs $\mathbf{R}$ [3], CA [4], CMOD [5], and DFT-Based [6] methods

Table 4.2: Comparison of MIMO Waveforms with respect to MSE, CDF, Cross Correlation, Bandwidth and Complexity

	MSE		CDF (%)	Σ XCorr	Bandwidth	Complexity	Computation time(s)
	Multi Beam	Single Beam	@-10 dB				
PCC-PAR	0.0359	0.0085	99.7	0.0424	Band-limited	$\mathcal{O}(M^3K^3) + \mathcal{O}(MK\log(K))$	8.72
$\mathbf{C}$ in [7]	-	0.0001	90.5	-	Band-limited	-	64.7
$\mathbf{S}$ in [5]	0.0385	0.0087	84.9	0.0438	-	$\mathcal{O}\left(M^3L^3\right)$	6.44
$\mathbf{R}$ in [3]	0.0353	0.0083	99.9	0.0241	-	$\mathcal{O}\left(M^{3.5}\right)$	3.25
$\mathbf{X}$ in [4]	0.0396	0.0115	99.6	0.0242	-	$\mathcal{O}\left(M^{3.5}\right) + \mathcal{O}\left(M^3\right)$	5.67
DFT-based [6]	0.202	0.105	-	-	-	$\mathcal{O}(M\log(M))$	0.28

4.4 Singlebeam Solutions

Similar performance characteristics are observed for the single beam case shown in Figure 4.5. The beamwidth for this case is $\Delta\theta = 60°$ centered at $\theta = 0°$. Beampattern shows more than 12.2 dB sidelobe supression under the most strict constraint $\delta = 1$.

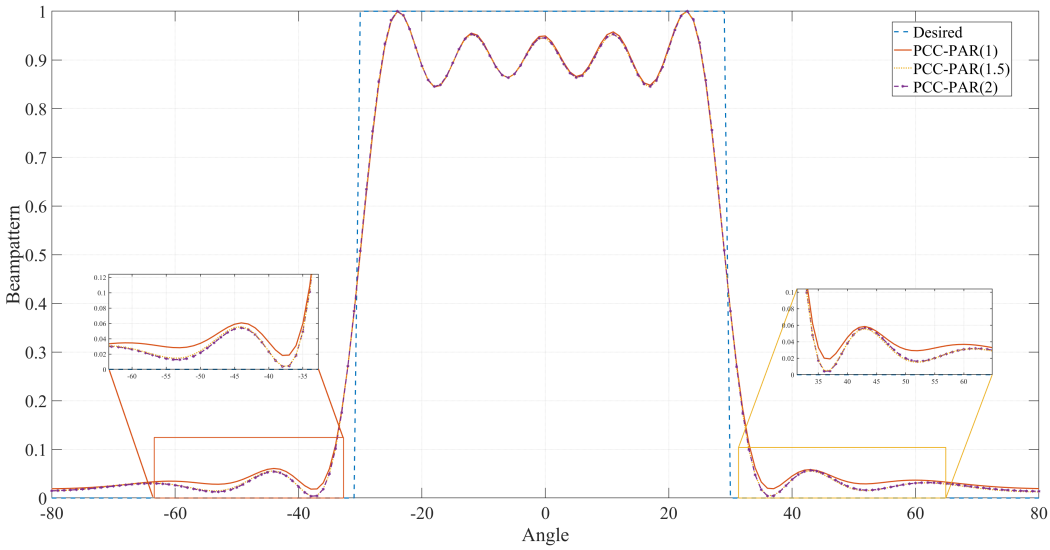

Figure 4.5: Single Beam PCC-PAR Solutions for $\delta = 1, 1.5, 2$

4.5 Optimized MIMO Ambiguity Function

Figure 4.6 and Figure 4.7 shows the 2D and 3D plots of generalized ambiguity function derived in (2.41) for $\tau = 0$ cut. Notice that the beampattern is placed on $\theta = \theta'$ line and cross terms is slightly noticable. Ambiguity function optimization reveals thumbstack shape for the desired target locations and suppresses sidelobes elsewhere, which greatly improves detection and resolution performance of the radar.

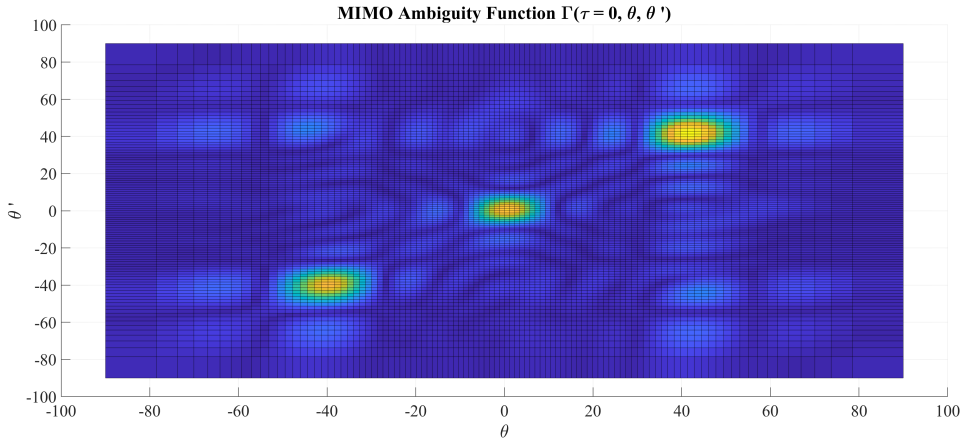

Figure 4.6: 2D Ambiguity Function cut for $\tau = 0$

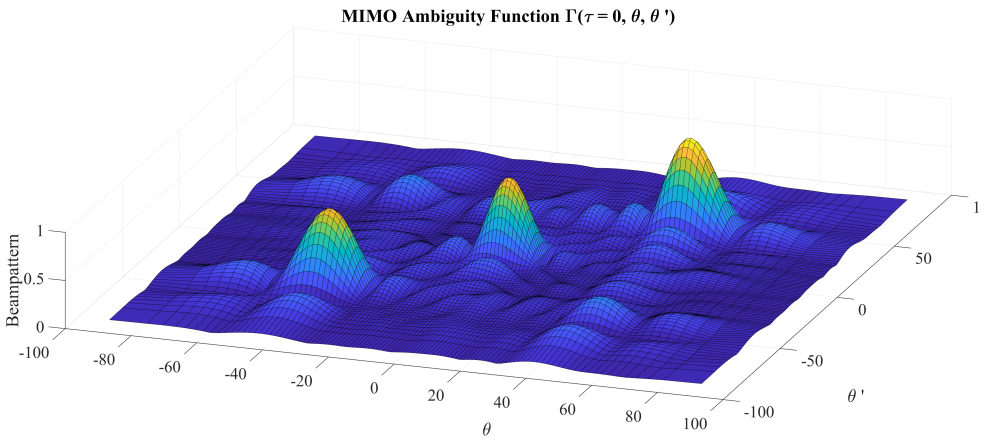

Figure 4.7: 3D Ambiguity Function cut for $\tau = 0$

4.6 CDF Distribution

A quantitative measure suggested by [7] is used for the effectiveness of Costas codes on different time lags and cross terms. Emprical cumulative distribution function (CDF) shows the percentage of the samples $|\Gamma(\tau, f, f')|$ less than relative magnitude with respect to the normalized peak. Figure 4.8 shows that PCC-PAR signal set gives very close performance to signal set derived from optimal covariance matrix $\mathbf{R}$. Both methods satisfy -20 dB or more supression on 94% while covariance method shows slightly superior for sidelobes greater than -20 dB. This result is expected since the samples from the optimal covariance matrix is produced using $\mathbf{x}(n) = \mathbf{R}^{1/2}\mathbf{w}(n)$ which is spectrally very spread. PCC-PAR achieves almost the same performance using limited bandwidth which has a significant practical importance.

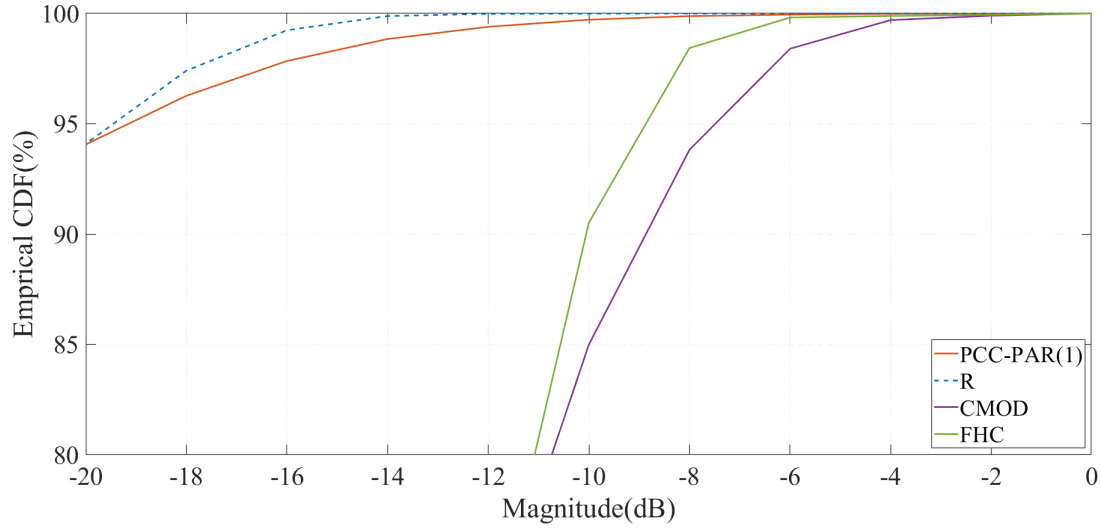

Figure 4.8: Emprical CDF performance of PCC-PAR(1), $\mathbf{R}$ [3], CMOD [5], FHC [7] methods

4.7 Spatial (Cross) Correlations

Figure 4.9 (a) shows the normalized cross correlation (4.1) results between all target combinations at fixed PAR with $\delta = 1$. The horizontal axis represents integer multiples of chip lengths kt_b. Notice that optimization reduces the spatial cross correlation below -20 dB while unoptimized case when $\sigma_c = 0$ leaves it -5dB. Figure 4.9 (b) shows the cross correlation between Target 1 and Target 2 under the varying PAR constraint. As the constraint is relaxed correlation at zero lag drops to a lower value (on the order of -30 dB when it is unconstrained) which is useful for data adaptive processing techniques. In both figures, notice that correlation value at zero lag depends on optimization of phase codes while nonzero lag values depends on Costas frequency code behavior.

$$|\Gamma(\tau,\theta,\theta')|_N = \frac{\left|\mathbf{a}^H(\theta)\mathbf{R}(\tau)\mathbf{a}(\theta')\right|}{\left[\mathbf{a}^H(\theta)\mathbf{R}(0)\mathbf{a}(\theta)\right]^{1/2}\left[\mathbf{a}^H(\theta')\mathbf{R}(0)\mathbf{a}(\theta')\right]^{1/2}} \tag{4.1}$$

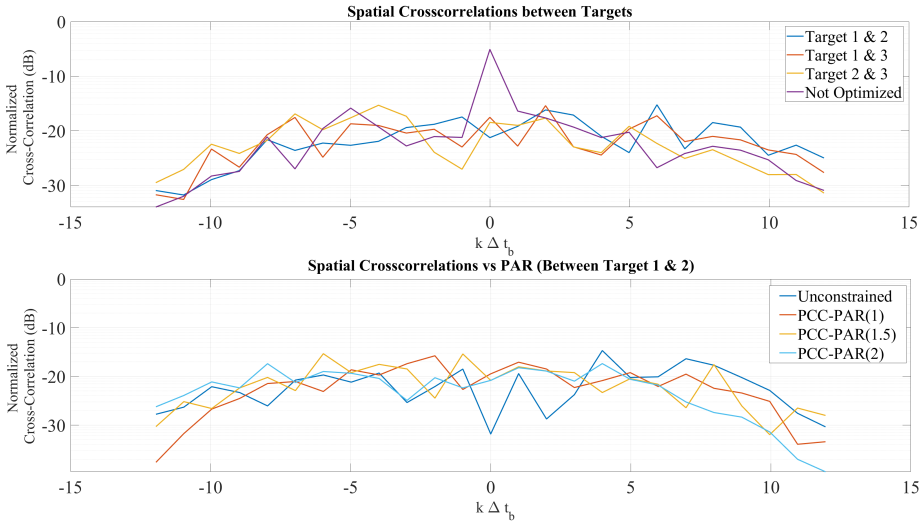

Figure 4.9: (a) Spatial Cross Correlation between multiple targets at fixed PAR with $\delta = 1$ (b) Spatial Cross Correlation between Target 1 and Target 2 with respect to different PAR values (δ)

4.8 Capon and GLRT Spectrums

For the three target scenario, radar cross section of targets is taken as unit value. Figure 4.10 and Figure 4.11 show the Capon and GLRT spectrum of received signal respectively. The waveform set for this case was PCC-PAR(1) coded with $K = 12$ chips. The received signal is corrupted with zero-mean circularly symmetric spatially and temporally white Gaussian noise with variance σ^2. The received signal model is given in (4.2). For each chip 256 samples created and using the data $\mathbf{y}(n)_{n=1}^{N}$ collected by the array for -20 dB SNR Capon and GLRT spectrums are found.

$$\mathbf{y}(n) = \sum_{l=1}^{L} \mathbf{a}^{C}(\theta_l)\mathbf{a}^{H}(\theta_l)\mathbf{x}(n) + \mathbf{w}(n) \tag{4.2}$$

- Capon spectrum is defined as:

$$\tilde{\phi}(\theta) = \frac{|\mathbf{a}^{H}(\theta)\hat{\mathbf{R}}_{yy}^{-1}\hat{\mathbf{R}}_{yx}\mathbf{a}^{C}(\theta)|}{[\mathbf{a}^{H}(\theta)\hat{\mathbf{R}}_{yy}^{-1}\mathbf{a}(\theta)][\mathbf{a}^{T}(\theta)\hat{\mathbf{R}}_{xx}\mathbf{a}^{C}(\theta)]} \tag{4.3}$$

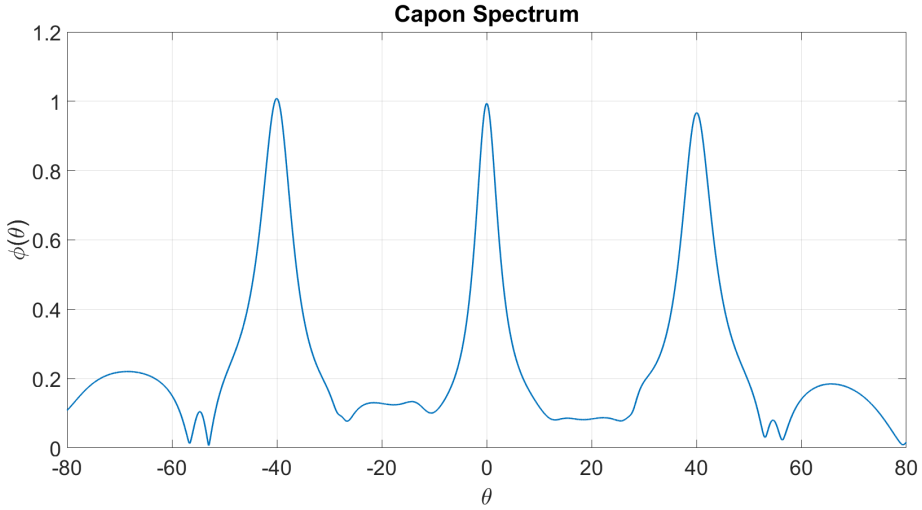

Figure 4.10: Capon Spectrum of Targets with -20 dB SNR

- From [14] GLRT technique is utilized for the spatial spectrum of the targets.

$$\tilde{\phi}(\theta) = 1 - \frac{\mathbf{a}^H(\theta)\hat{\mathbf{R}}_{yy}^{-1}\mathbf{a}(\theta)}{\mathbf{a}^H(\theta)\hat{\mathbf{Q}}^{-1}\mathbf{a}(\theta)} \tag{4.4}$$

$$\hat{\mathbf{Q}} = \hat{\mathbf{R}}_{yy} - \frac{\hat{\mathbf{R}}_{yx}\mathbf{a}(\theta)\mathbf{a}^H(\theta)\hat{\mathbf{R}}_{yx}^H}{\mathbf{a}^H(\theta)\hat{\mathbf{R}}_{xx}\mathbf{a}(\theta)} \tag{4.5}$$

$$\hat{\mathbf{R}}_{yx} = \frac{1}{N}\sum_{n=1}^{N}\mathbf{y}(n)\mathbf{x}^H(n) \tag{4.6}$$

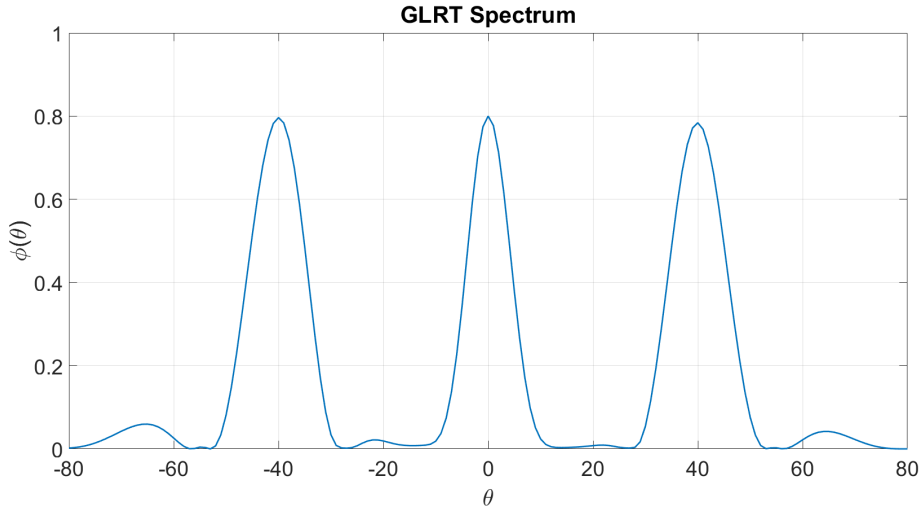

Figure 4.11: GLRT Spectrum of Targets with -20 dB SNR

CHAPTER 5

CONCLUSION

5.1 Summary and Results

In this thesis, a simple formulation for the generalized ambiguity function is derived and employed for the design of multiple constraint MIMO radar beamformer. The advantage of this new formulation is its simplicity compared to previous formulations in order to observe several characteristics of the beamformer which also leads to simple optimization problems. Several practical desired features for a MIMO radar beamformer are outlined. We proposed a modified Phased-Costas coded sequences for MIMO waveforms where frequency coding in time and phase coding in space are used to satisfy the low range sidelobes and target cross-correlations. These waveforms are also bandlimited making it suitable for conventional radar applications. The beamformer design problem is outlined as a constained optimization problem to obtain a desired beampattern with low PAR constraint. This problem is nonconvex and NP hard. It is converted to a convex problem and solved through ADMM method to obtain the optimum solution with any desired PAR value. An efficient solution is presented to reduce the computational complexity. This work presents a solution for nonlinear amplifier structures which require constant modulus signals for low distortion in MIMO radar context. It is shown that even $PAR = 1$ can be achieved with little loss in beampattern shape compared to unconstrained problem. Several simulations are done to compare the proposed solution with the previous works. It is shown that the presented approach has better characteristics in terms of several desired features including PAR, bandwidth, auto/cross correlations and cumulative distribution functions.

5.2 Further Works

In this thesis, we decouple the temporal requirement of waveforms (optimizing range sidelobes) using inherent orthogonality properties of Costas coded waveforms, and satisfy beampattern related constraints using the phase codes. In a further study, it might be possible to attempt the optimization of ambiguity function without decoupling. This requires combining spectral limitations (in terms of bandwidth and/or range-sidelobe levels) of waveforms during beamformer optimization. This method might remove frequency hopping of the chips and realize necessary requirements with a different waveform set.

REFERENCES

[1] J. Li and P. Stoica, "MIMO Radar with Colocated Antennas," *IEEE Signal Processing Magazine*, vol. 24, no. 5, pp. 106–114, 2007.

[2] N. Levanon and E. Mozeson, *Radar Signals*. 2004.

[3] P. Stoica, J. Li, and Y. Xie, "On probing signal design for MIMO radar," *IEEE Transactions on Signal Processing*, vol. 55, no. 8, pp. 4151–4161, 2007.

[4] P. Stoica, J. Li, and X. Zhu, "Waveform synthesis for diversity-based transmit beampattern design," *IEEE Transactions on Signal Processing*, vol. 56, no. 6, pp. 2593–2598, 2008.

[5] Z. Cheng, Z. He, S. Zhang, and J. Li, "Constant Modulus Waveform Design for MIMO Radar Transmit Beampattern," *IEEE Transactions on Signal Processing*, vol. 65, no. 18, pp. 4912–4923, 2017.

[6] T. Bouchoucha, S. Ahmed, T. Al-Naffouri, and M. S. Alouini, "DFT-Based Closed-Form Covariance Matrix and Direct Waveforms Design for MIMO Radar to Achieve Desired Beampatterns," *IEEE Transactions on Signal Processing*, vol. 65, no. 8, pp. 2104–2113, 2017.

[7] C. Y. Chen and P. P. Vaidyanathan, "MIMO radar ambiguity properties and optimization using frequency-hopping waveforms," *IEEE Transactions on Signal Processing*, vol. 56, no. 12, pp. 5926–5936, 2008.

[8] Y. Wang, Y. Wang, and Q. Shi, "Optimized signal distortion for PAPR reduction of OFDM signals with IFFT/FFT complexity via ADMM approaches," *IEEE Transactions on Signal Processing*, vol. 67, no. 2, pp. 399–414, 2019.

[9] A. M. Haimovich, R. S. Blum, and L. J. Cimini, "MIMO radar with widely separated antennas," 2008.

[10] E. Fishler, A. Haimovich, R. S. Blum, L. J. Cimini, D. Chizhik, and R. A. Valenzuela, "Spatial diversity in radars - Models and detection performance," *IEEE Transactions on Signal Processing*, vol. 54, no. 3, pp. 823–838, 2006.

[11] D. W. Bliss and K. W. Forsythe, "Multiple-input multiple-output (MIMO) radar and imaging: Degrees of freedom and resolution," *Conference Record of the Asilomar Conference on Signals, Systems and Computers*, vol. 1, pp. 54–59, 2003.

[12] K. W. Forsythe, D. W. Bliss, and G. S. Fawcett, "Multiple-Input Multiple-Output (MIMO) radar: Performance issues," *Conference Record - Asilomar Conference on Signals, Systems and Computers*, vol. 1, pp. 310–315, 2004.

[13] J. Li, P. Stoica, L. Xu, and W. Roberts, "On parameter identifiability of MIMO radar," *IEEE Signal Processing Letters*, vol. 14, no. 12, pp. 968–971, 2007.

[14] L. Xu, J. Li, and P. Stoica, "Radar imaging via adaptive MIMO techniques," in *European Signal Processing Conference*, no. Eusipco, pp. 37–46, 2006.

[15] O. Aldayel, V. Monga, and M. Rangaswamy, "Successive QCQP Refinement for MIMO Radar Waveform Design under Practical Constraints," *IEEE Transactions on Signal Processing*, vol. 64, no. 14, pp. 3760–3774, 2016.

[16] Y. Yang and R. S. Blum, "Waveform design for MIMO radar based on mutual information and minimum mean-square error estimation," *2006 IEEE Conference on Information Sciences and Systems, CISS 2006 - Proceedings*, pp. 111–116, 2006.

[17] Y. Yang and R. S. Blum, "Minimax robust MIMO radar waveform design," *IEEE Journal on Selected Topics in Signal Processing*, vol. 1, no. 1, pp. 147–155, 2007.

[18] A. Leshem, O. Naparstek, and A. Nehorai, "Information theoretic adaptive radar waveform design for multiple extended targets," *IEEE Journal on Selected Topics in Signal Processing*, vol. 1, no. 1, pp. 42–55, 2007.

[19] C. Y. Chen and P. P. Vaidyanathan, "MIMO radar waveform optimization with prior information of the extended target and clutter," *IEEE Transactions on Signal Processing*, vol. 57, no. 9, pp. 3533–3544, 2009.

[20] G. Cui, H. Li, and M. Rangaswamy, "MIMO radar waveform design with constant modulus and similarity constraints," *IEEE Transactions on Signal Processing*, vol. 62, no. 2, pp. 343–353, 2014.

[21] Z. Q. Luo, W. K. Ma, A. So, Y. Ye, and S. Zhang, "Semidefinite relaxation of quadratic optimization problems," *IEEE Signal Processing Magazine*, vol. 27, no. 3, pp. 20–34, 2010.

[22] B. Tang, J. Tuck, and P. Stoica, "Polyphase Waveform Design for MIMO Radar Space Time Adaptive Processing," *IEEE Transactions on Signal Processing*, vol. 68, pp. 2170–2181, 2020.

[23] B. Tang and J. Tang, "Joint Design of Transmit Waveforms and Receive Filters for MIMO Radar Space-Time Adaptive Processing," *IEEE Transactions on Signal Processing*, vol. 64, no. 18, pp. 4707–4722, 2016.

[24] G. Cui, X. Yu, V. Carotenuto, and L. Kong, "Space-Time Transmit Code and Receive Filter Design for Colocated MIMO Radar," *IEEE Transactions on Signal Processing*, vol. 65, no. 5, pp. 1116–1129, 2017.

[25] X. Yu, G. Cui, L. Kong, J. Li, and G. Gui, "Constrained waveform design for colocated MIMO radar with uncertain steering matrices," *IEEE Transactions on Aerospace and Electronic Systems*, vol. 55, no. 1, pp. 356–370, 2019.

[26] S. Shi, Z. He, and Z. Wang, "Joint Design of Transmitting Waveforms and Receiving Filter for MIMO-STAP Airborne Radar," *Circuits, Systems, and Signal Processing*, vol. 39, no. 3, pp. 1489–1508, 2020.

[27] P. Stoica, H. He, and J. Li, "New algorithms for designing unimodular sequences with good correlation properties," *IEEE Transactions on Signal Processing*, vol. 57, no. 4, pp. 1415–1425, 2009.

[28] H. He, P. Stoica, and J. Li, "Designing unimodular sequence sets with good correlations - Including an application to MIMO radar," *IEEE Transactions on Signal Processing*, vol. 57, no. 11, pp. 4391–4405, 2009.

[29] D. R. Fuhrmann and G. San Antonio, "Transmit beamforming for MIMO radar systems using signal cross-correlation," *IEEE Transactions on Aerospace and Electronic Systems*, vol. 44, no. 1, pp. 171–186, 2008.

[30] J. Li, P. Stoica, and X. Zheng, "Signal synthesis and receiver design for MIMO radar imaging," *IEEE Transactions on Signal Processing*, vol. 56, no. 8 II, pp. 3959–3968, 2008.

[31] A. De Maio, Y. Huang, M. Piezzo, S. Zhang, and A. Farina, "Design of optimized radar codes with a peak to average power ratio constraint," *IEEE Transactions on Signal Processing*, vol. 59, no. 6, pp. 2683–2697, 2011.

[32] Q. He, N. H. Lehmann, R. S. Blum, and A. M. Haimovich, "MIMO radar moving target detection in homogeneous clutter," *IEEE Transactions on Aerospace and Electronic Systems*, vol. 46, no. 3, pp. 1290–1301, 2010.

[33] N. H. Lehmann, A. M. Haimovich, R. S. Blum, and L. Cimini, "High resolution capabilities of MIMO radar," *Conference Record - Asilomar Conference on Signals, Systems and Computers*, pp. 25–30, 2006.

[34] E. Fishler, A. Haimovich, R. Blum, D. Chizhik, L. Cimini, and R. Valenzuela, "MIMO radar: An idea whose time has come," in *IEEE National Radar Conference - Proceedings*, pp. 71–78, 2004.

[35] N. H. Lehmann, E. Fishler, A. M. Haimovich, R. S. Blum, D. Chizhik, L. J. Cimini, and R. A. Valenzuela, "Evaluation of transmit diversity in MIMO-radar direction finding," *IEEE Transactions on Signal Processing*, vol. 55, no. 5 II, pp. 2215–2225, 2007.

[36] P. Stoica and G. Ganesan, "Maximum-SNR spatial-temporal formatting designs for MIMO channels," *IEEE Transactions on Signal Processing*, vol. 50, no. 12, pp. 3036–3042, 2002.

[37] G. San Antonio, D. R. Fuhrmann, and F. C. Robey, "MIMO radar ambiguity functions," *IEEE Journal on Selected Topics in Signal Processing*, vol. 1, no. 1, pp. 167–177, 2007.

[38] Y. Li, S. A. Vorobyov, and V. Koivunen, "Generalized ambiguity function for the MIMO radar with correlated waveforms," *ICASSP, IEEE International Conference on Acoustics, Speech and Signal Processing - Proceedings*, pp. 5302–5306, 2014.

[39] M. A. Richards, J. A. Scheer, and W. A. Holm, *Principles of modern radar: Basic principles*. 2010.

[40] J. Silverman, V. E. Vickers, and J. M. Mooney, "On the number of costas arrays as a function of array size," *Proceedings of the IEEE*, vol. 76, no. 7, pp. 851–853, 1988.

[41] S. W. Golomb and H. Taylor, "Constructions and Properties of Costas Arrays," *Proceedings of the IEEE*, vol. 72, no. 9, pp. 1143–1163, 1984.

[42] Ö. Çayır and Ç. Candan, "Transmit beamformer design with a PAPR constraint to trade-off between beampattern shape and power efficiency," *Digital Signal Processing: A Review Journal*, vol. 99, 2020.

[43] S. Boyd, N. Parikh, E. Chu, B. Peleato, and J. Eckstein, *Distributed optimization and statistical learning via the alternating direction method of multipliers*, vol. 3. 2010.

[44] S. Boyd, S. P. Boyd, and L. Vandenberghe, *Convex optimization*. Cambridge university press, 2004.

APPENDIX A

BINARY SEARCH OF LAGRANGIAN MULTIPLER

Algorithm 2: Binary Search of Lagrangian Multipler [8]

Input: Search boundary (γ^k_{left}, γ^k_{right})

Output: γ^{k*}

repeat

  $\gamma^k = \frac{\gamma^k_{\text{left}}+\gamma^k_{\text{right}}}{2}$;

  Update $\tilde{\mathbf{s}}^{k+1}$ using (3.57) ;

  if $\|\tilde{\mathbf{s}}^{k+1}\|^2 < 1$ **then**

    $\gamma^k_{\text{right}} = \gamma^k$;

  else

    $\gamma^k_{\text{left}} = \gamma^k$;

  end

until *(*$\|\tilde{\mathbf{s}}^{k+1}\|^2 \approx 1$*)*;

$\gamma^{k*} = \frac{\gamma^k_{\text{left}}+\gamma^k_{\text{right}}}{2}$;

APPENDIX B

CLOSED FORM EXPRESSIONS OF UPDATE EQUATIONS

B.1 Update of $\mathbf{v}_1^{m+1}$

$$\mathbf{v}_1^{m+1} := \arg\min_{\mathbf{v}_1} \mathcal{L}\left(\mathbf{v_1}, \mathbf{v_2}^m, \mathbf{q_1}^{m+1}, \mathbf{q_2}^{m+1}, \mathbf{u}^m, \mathbf{w}^m, \mathbf{z}^m\right)$$

Closed form expressions for (3.51c) is found by setting gradient of augmented Lagrangian to zero with respect to $\mathbf{v}_1$. Expanding $F(\mathbf{v}_1, \mathbf{v}_2)$ and using definition in (3.58b) for $\mathbf{C}_1$ we have

$$\begin{aligned}\mathbf{0} = \nabla_{\mathbf{v}_1}\Big(&\mathbf{v}_1^H\mathbf{C}_1\,\mathbf{v}_1 + \frac{\rho_1}{2}\|\mathbf{v}_1 - \mathbf{v}_2^m + \mathbf{u}^m\|^2 \\ &+\frac{\rho_2}{2}\|\mathbf{E}\mathbf{v}_1 - \mathbf{q}_1^{m+1} + \mathbf{w}^m\|^2 + \frac{\rho_3}{2}\|\mathbf{E}\mathbf{v}_2 - \mathbf{q}_2^{m+1} + \mathbf{z}^m\|^2\Big)\end{aligned} \tag{B.1}$$

Defining each term in (B.1) as (B.2)-(B.5), augmented Lagrangian can be written as (B.6).

$$\mathcal{L}_1 \triangleq \mathbf{v}_1^H\mathbf{C}_1\,\mathbf{v}_1 \tag{B.2}$$

$$\mathcal{L}_2 \triangleq \frac{\rho_1}{2}\|\mathbf{v}_1 - \mathbf{v}_2^m + \mathbf{u}^m\|^2 \tag{B.3}$$

$$\mathcal{L}_3 \triangleq \frac{\rho_2}{2}\|\mathbf{E}\mathbf{v}_1 - \mathbf{q}_1^{m+1} + \mathbf{w}^m\|^2 \tag{B.4}$$

$$\mathcal{L}_4 \triangleq \frac{\rho_3}{2}\|\mathbf{E}\mathbf{v}_2 - \mathbf{q}_2^{m+1} + \mathbf{z}^m\|^2 \tag{B.5}$$

$$\mathcal{L} = \mathcal{L}_1 + \mathcal{L}_2 + \mathcal{L}_3 + \mathcal{L}_4 \tag{B.6}$$

Writing $\mathbf{v}_1$ in terms of its real and imaginary parts $\mathbf{p} = [\mathrm{Re}(\mathbf{v}_1); \mathrm{Im}(\mathbf{v}_1)]$ and using chain rule gives

$$\nabla_{\mathbf{p}}\mathcal{L}_1 = \left(\frac{\partial\mathbf{v}_1}{\partial\mathbf{p}}\right)^C \mathbf{C}_1\mathbf{v}_1 + \frac{\partial\mathbf{v}_1}{\partial\mathbf{p}}\mathbf{C}_1^T\mathbf{v}_1^C \tag{B.7}$$

$$\nabla_{\mathbf{p}}\mathcal{L}_2 = \frac{\rho_1}{2}\cdot\left[\left(\frac{\partial \mathbf{v}_1}{\partial \mathbf{p}}\right)^C(\mathbf{v}_1 - \mathbf{v}_2^m + \mathbf{u}^m) + \frac{\partial \mathbf{v}_1}{\partial \mathbf{p}}(\mathbf{v}_1 - \mathbf{v}_2^m + \mathbf{u}^m)^C\right] \tag{B.8}$$

$$\nabla_{\mathbf{p}}\mathcal{L}_3 = \frac{\rho_2}{2}\cdot\left[\left(\frac{\partial \mathbf{E}\mathbf{v}_1}{\partial \mathbf{p}}\right)^C(\mathbf{E}\mathbf{v}_1 - \mathbf{q}_1^m + \mathbf{w}^m) + \frac{\partial \mathbf{E}\mathbf{v}_1}{\partial \mathbf{p}}(\mathbf{E}\mathbf{v}_1 - \mathbf{q}_1^m + \mathbf{w}^m)^C\right]$$

$$= \frac{\rho_2}{2}\cdot\left[\left(\frac{\partial \mathbf{v}_1}{\partial \mathbf{p}}\right)^C\mathbf{E}^T(\mathbf{E}\mathbf{v}_1 - \mathbf{q}_1^m + \mathbf{w}^m) + \frac{\partial \mathbf{v}_1}{\partial \mathbf{p}}\mathbf{E}^T(\mathbf{E}\mathbf{v}_1 - \mathbf{q}_1^m + \mathbf{w}^m)^C\right] \tag{B.9}$$

$$\nabla_{\mathbf{p}}\mathcal{L}_4 = \mathbf{0} \tag{B.10}$$

Note that $\mathbf{C_1} = \mathbf{C_1}^H$ is hermitian symmetric and inner terms in each Lagrangian (B.7)-(B.10) is conjugate of each other. Also notice that first element(scaling coefficient α) of $\mathbf{v}_1$ is not included in optimization of $\mathcal{L}_3$. Expressing $\mathbf{E}^T = [\mathbf{0}; \mathbf{I}]$ previously defined in (3.24) the summation becomes

$$\begin{aligned}
&\nabla_{\mathbf{p}}\ \mathcal{L}_1 + \mathcal{L}_2 + \mathcal{L}_3 + \mathcal{L}_4 \\
&\quad = 2\,\mathrm{Re}\left\{\left(\frac{\partial \mathbf{v}_1}{\partial \mathbf{p}}\right)^C\mathbf{C}_1\mathbf{v}_1 + \frac{\rho_1}{2}\cdot\left[\left(\frac{\partial \mathbf{v}_1}{\partial \mathbf{p}}\right)^C(\mathbf{v}_1 - \mathbf{v}_2^m + \mathbf{u}^m)\right]\right. \\
&\qquad \left. + \frac{\rho_2}{2}\cdot\left[\left(\frac{\partial \mathbf{v}_1}{\partial \mathbf{p}}\right)^C\begin{bmatrix}0\\ \mathbf{I}\end{bmatrix}(\mathbf{E}\mathbf{v}_1 - \mathbf{q}_1^{m+1} + \mathbf{w}^m)\right]\right\} \\
&\quad = 2\,\mathrm{Re}\left\{\left(\frac{\partial \mathbf{v}_1}{\partial \mathbf{p}}\right)^C\left\{\left(\mathbf{C_1} + \frac{\rho_1}{2}\mathbf{I} + \frac{\rho_2}{2}\begin{bmatrix}0\\ \mathbf{E}\end{bmatrix}\right)\mathbf{v}_1\right.\right. \\
&\qquad \left.\left. - \left(\frac{\rho_1}{2}(\mathbf{v_2}^m - \mathbf{u}^m) + \begin{bmatrix}0\\ \frac{\rho_2}{2}(\mathbf{q_1}^{m+1} - \mathbf{w}^m)\end{bmatrix}\right)\right\}\right\}
\end{aligned} \tag{B.11}$$

Equating inner term in (B.11) to $\mathbf{0}$ and leaving $\mathbf{v}_1$ on the left side

$$\left(\mathbf{C_1} + \frac{\rho_1}{2}\mathbf{I} + \frac{\rho_2}{2}\begin{bmatrix} 0 \\ \mathbf{E} \end{bmatrix}\right)\mathbf{v}_1 = \left(\frac{\rho_1}{2}(\mathbf{v_2}^m - \mathbf{u}^m) + \begin{bmatrix} 0 \\ \frac{\rho_2}{2}(\mathbf{q_1}^{m+1} - \mathbf{w}^m) \end{bmatrix}\right) \tag{B.12}$$

Therefore, $\mathbf{v}_1^{m+1}$ is found as

$$\mathbf{v_1^{m+1}} = \left(\mathbf{C_1} + \frac{\rho_1}{2}\mathbf{I} + \frac{\rho_2}{2}\begin{bmatrix} 0 \\ \mathbf{E} \end{bmatrix}\right)^{-1} \left(\frac{\rho_1}{2}(\mathbf{v_2}^m - \mathbf{u}^m) + \begin{bmatrix} 0 \\ \frac{\rho_2}{2}(\mathbf{q_1}^{m+1} - \mathbf{w}^m) \end{bmatrix}\right) \tag{B.13}$$

B.2 Update of $\mathbf{v}_2^{m+1}$

$$\mathbf{v}_2^{m+1} := \arg\min_{\mathbf{v_2}} \mathcal{L}\left(\mathbf{v_1}^{m+1}, \mathbf{v_2}, \mathbf{q_1}^{m+1}, \mathbf{q_2}^{m+1}, \mathbf{u}^m, \mathbf{w}^m, \mathbf{z}^m\right)$$

Similarly for $\mathbf{v}_2$ with $\nabla_{\mathbf{p}}\mathcal{L}_3 = \mathbf{0}$ and $\nabla_{\mathbf{p}}\mathcal{L}_4$ nonzero, same steps are applied after the update of $\mathbf{v}_1^{m+1}$. Expanding $F(\mathbf{v}_1, \mathbf{v}_2)$ and using definition in (3.59b) for $\mathbf{C}_2$ we have closed form solution found as

$$\left(\mathbf{C_2} + \frac{\rho_1}{2}\mathbf{I} + \frac{\rho_3}{2}\begin{bmatrix} 0 \\ \mathbf{E} \end{bmatrix}\right)\mathbf{v}_2 = \left(\frac{\rho_1}{2}(\mathbf{v_1}^{m+1} + \mathbf{u}^m) + \begin{bmatrix} 0 \\ \frac{\rho_3}{2}(\mathbf{q_2}^{m+1} - \mathbf{z}^m) \end{bmatrix}\right) \tag{B.14}$$

$$\mathbf{v_2^{m+1}} = \left(\mathbf{C_2} + \frac{\rho_1}{2}\mathbf{I} + \frac{\rho_3}{2}\begin{bmatrix} 0 \\ \mathbf{E} \end{bmatrix}\right)^{-1} \left(\frac{\rho_1}{2}(\mathbf{v_1}^{m+1} + \mathbf{u}^m) + \begin{bmatrix} 0 \\ \frac{\rho_3}{2}(\mathbf{q_2}^{m+1} - \mathbf{z}^m) \end{bmatrix}\right) \tag{B.15}$$

APPENDIX C

BI-CONVEXITY OF COST FUNCTION IN ADMM FORM

$$J = \mathbf{v}^H \mathbf{A}(\theta_k)\mathbf{v} \tag{C.1}$$

$$\nabla J(\mathbf{v}) = (\mathbf{A} + \mathbf{A}^H)\mathbf{v} \tag{C.2}$$

$$\nabla^2 J(\mathbf{v}) = (\mathbf{A} + \mathbf{A}^H) \tag{C.3}$$

Therefore Hessian is not positive semidefinite due to $\mathbf{A}$ defined in (3.17). However if we seperate the function to two primal variables as

$$\mathbf{v}^H \mathbf{A}(\theta_k)\mathbf{v} = \mathbf{v}_1^H \mathbf{A}(\theta_k)\mathbf{v}_2 \tag{C.4}$$

$$\tag{C.5}$$

It becomes bi-convex (i.e when $\mathbf{v}_1$ is fixed, Hessian becomes $\mathbf{0}$) and vice versa.

$$\text{Let } \mathbf{a}^H = \mathbf{v}_1^H \mathbf{A}(\theta_k) \tag{C.6}$$

$$J = \mathbf{a}^H \mathbf{v}_2 \tag{C.7}$$

$$\nabla J(\mathbf{v}) = \mathbf{a} \tag{C.8}$$

$$\nabla^2 J(\mathbf{v}) = \mathbf{0} \tag{C.9}$$

APPENDIX D

SUBOPTIMUM AND VARYING POWER APPROACHES

D.1 Suboptimum Methods (PCC-SUB)

Suboptimum solutions can be derived without integrating PAR constraints in ADMM formulation. The nearest vector with desired PAR to the resulting samples at the end of ADMM optimization (satisfying beampattern and low cross correlation constraints) can be found similarly. However multibeam and singlebeam performance of this method drops significantly as shown in Figure D.1 and Figure D.2. Notice that in Figure D.1, the optimum solution is given in PCC-PAR(1) and suboptimum solutions are denoted as PCC-SUB(δ). As PAR constraint is relaxed (δ increasing) suboptimum solutions are getting closer to the PCC-PAR solution.

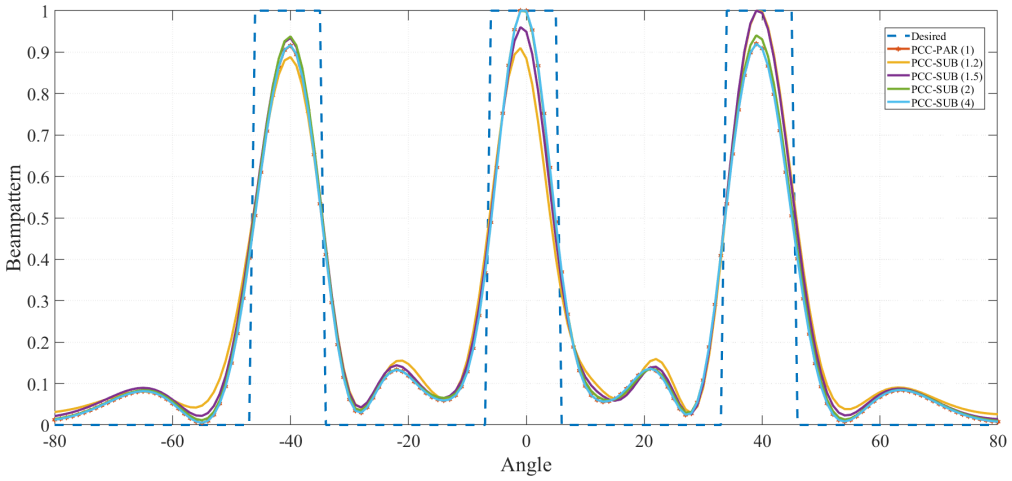

Figure D.1: Multi Beam PCC-SUB Solutions for $\delta = 1.2, 1.5, 2, 4$

The inferiority of the suboptimum approach becomes more obvious in the single beam

case. In Figure D.2 PCC-SUB(1) solution deviates considerably from the optimum PCC-PAR(1) case.

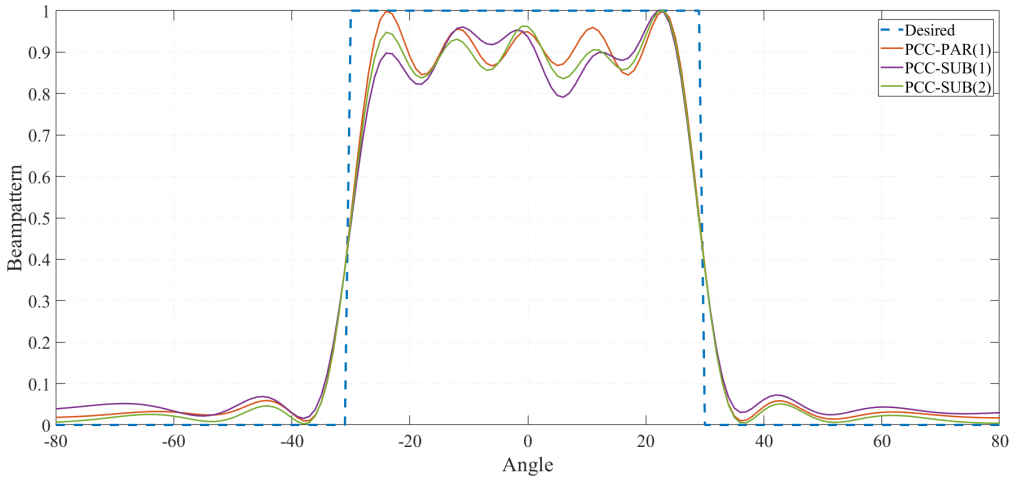

Figure D.2: Single Beam PCC-SUB Solutions for $\delta = 1, 2$

D.2 Varying Power Case

Apart from the suboptimality, we also tested the performance when we let the power of each waveform flexible during the optimization. It turns out that in Figure D.3 the difference is only negligible in terms of the beampattern shapes. Therefore it is desirable to fix same power to the waveforms for uniformity of power amplifiers.

Figure D.4 and Figure D.5 shows the envelopes of the varying and constant power waveforms under PAR(1) constraint.

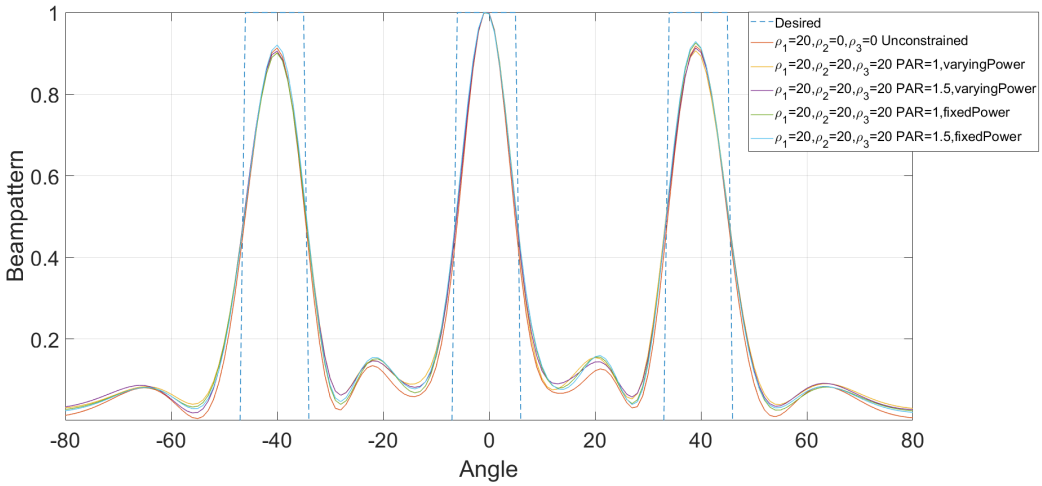

Figure D.3: Beampattern with respect to Varying and Constant Power $\delta = 1, 2$

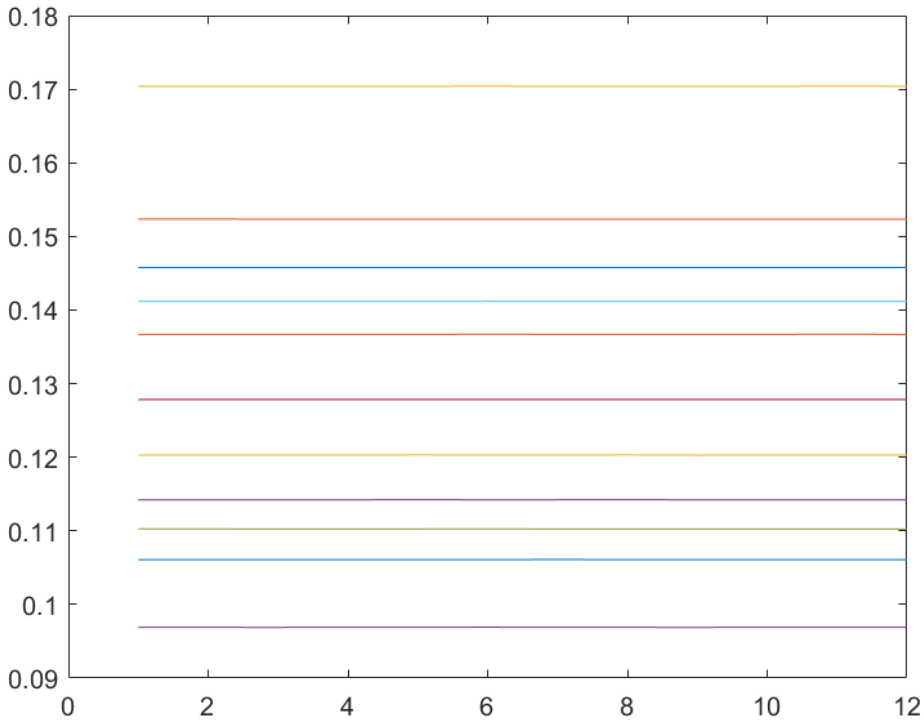

Figure D.4: Envelopes of the waveforms with Varying Power and PAR(1)

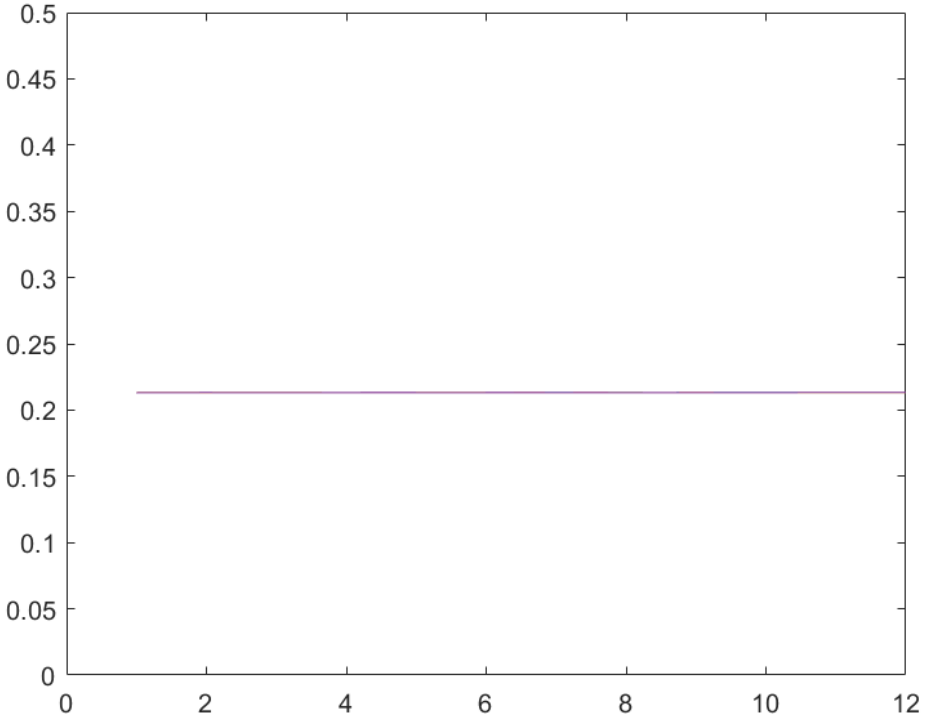

Figure D.5: Envelopes of the waveforms with Constant (Same) Power and PAR(1)